DEVELOPMENT OF IMPEDANCE FLOW CYTOMETRY SYSTEM FOR WHITE BLOOD CELL COUNT

A THESIS SUBMITTED TO
THE GRADUATE SCHOOL OF NATURAL AND APPLIED SCIENCES
OF
MIDDLE EAST TECHNICAL UNIVERSITY

BY

MEHMET ALPER DEMİR

IN PARTIAL FULFILLMENT OF THE REQUIREMENTS
FOR
THE DEGREE OF MASTER OF SCIENCE
IN
MICRO AND NANOTECHNOLOGY

JANUARY 2023

Approval of the thesis:

DEVELOPMENT OF IMPEDANCE FLOW CYTOMETRY SYSTEM FOR WHITE BLOOD CELL COUNT

submitted by **MEHMET ALPER DEMİR** in partial fulfillment of the requirements for the degree of **Master of Science** i**n Micro and Nanotechnology, Middle East Technical University** by,

Prof. Dr. Halil Kalıpçılar
Dean, Graduate School of **Natural and Applied Sciences** _____

Prof. Dr. Deniz Üner
Head of the Department, **Micro and Nanotechnology** _____

Prof. Dr. Haluk Külah
Supervisor, **Micro and Nanotechnology, METU** _____

Assoc. Prof. Dr. Ender Yıldırım
Co-Supervisor, **Mechanical Eng. Dept., METU** _____

Examining Committee Members:

Asst. Prof. Altuğ Özçelikkale
Mechanical Eng. Dept., METU _____

Prof. Dr. Haluk Külah
Micro and Nanotechnology, METU _____

Assoc. Prof. Dr. Ender Yıldırım
Mechanical Eng. Dept., METU _____

Prof. Dr. Uğur Tamer
Analytical Chemistry Dept., Gazi Uni. _____

Assoc. Prof. Dr. Hüseyin Cumhur Tekin
Bioengineering Dept., İYTE _____

Date: 26.01.2023

I hereby declare that all information in this document has been obtained and presented in accordance with academic rules and ethical conduct. I also declare that, as required by these rules and conduct, I have fully cited and referenced all material and results that are not original to this work.

Name Last name : Mehmet Alper Demir

Signature :

ABSTRACT

DEVELOPMENT OF IMPEDANCE FLOW CYTOMETRY SYSTEM FOR WHITE BLOOD CELL COUNT

Demir, Mehmet Alper
Master of Science, Micro and Nanotechnology
Supervisor: Prof. Dr. Haluk Külah
Co-Supervisor: Assoc. Prof. Dr. Ender Yıldırım

January 2023, 96 pages

White blood cells (WBCs) play a critical role in fighting infections. An increase in the WBC level can indicate the presence of an infection, and the ratio of neutrophils to lymphocytes can provide insight into the type of infection. A higher neutrophil to lymphocyte count ratio suggests a bacterial infection. Accurate identification of the infection's origin is important to ensure proper treatment and avoid contributing to the growing issue of antibiotic resistance.

A need for a system that offers accessibility and fast results exists in this field. Market systems deliver reliable results but may not be accessible due to their high costs. Instead, cell characterization based on electrical field response variations at different frequencies has been shown to be a alternative to available systems. This method depends on the characteristics of cells, such as cell membrane and cytoplasm.

In this thesis, using the impedance flow cytometry technique, a microfluidic cell counting chip that determines the neutrophil / lymphocyte ratio in a sample is designed and characterized. Enumaration and differentiation between two cell groups is achieved. Experiment results give a promising outlook for developing of a cost-effective cell counter system that provides fast results.

Keywords: Impedance Flow Cytometry, Cell Counting

ÖZ

BEYAZ KAN HÜCRESİ SAYIMI İÇİN EMPEDANS AKIŞ SİTOMETRİSİ SİSTEMİ GELİŞTİRİLMESİ

Demir, Mehmet Alper
Yüksek Lisans, Mikro ve Nanoteknoloji
Tez Yöneticisi: Prof. Dr. Haluk Külah
Ortak Tez Yöneticisi: Doç. Dr. Ender Yıldırım

Ocak 2023, 96 sayfa

Akyuvarlar enfeksiyonlarla mücadelede kritik bir rol oynar. Akyuvar seviyesindeki bir artış, bir enfeksiyonun varlığını gösterebilir ve nötrofillerin lenfositlere oranı, enfeksiyonun türü hakkında fikir verebilir. Daha yüksek bir nötrofil/lenfosit sayısı oranı bakteriyel bir enfeksiyonu düşündürür. Enfeksiyonun kaynağının doğru bir şekilde tanımlanması, uygun tedaviyi sağlamak ve büyüyen antibiyotik direnci sorununa katkıda bulunmaktan kaçınmak için önemlidir.

Bu alanda erişilebilir olan ve hızlı sonuç veren bir sisteme ihtiyaç vardır. Piyasadaki sistemler güvenilir sonuçlar verebilir ancak yüksek maliyetleri nedeniyle erişilebilir olmayabilir. Bunun yerine, farklı frekanslardaki elektrik alan yanıtı varyasyonlarına dayanan hücre karakterizasyonunun, mevcut sistemlere bir alternatif olduğu gösterilmiştir. Bu yöntem, hücre zarı ve sitoplazma gibi hücrelerin özelliklerine bağlı olarak bir karakterizasyon sağlar.

Bu tezde, empedans akış sitometri tekniği kullanılarak, bir numunede nötrofil/lenfosit oranını belirleyen bir mikroakışkan hücre sayma çipi tasarlanmış ve karakterize edilmiştir. İki hücre grubu için sayma ve farklılaşma sağlanmıştır. Deney

sonuçları, hızlı sonuç sağlayan uygun maliyetli bir hücre sayaç sisteminin geliştirilmesi için umut verici bir görünüm vermiştir.

Anahtar Kelimeler: Empedans Akış Sitometrisi, Hücre Sayımı

To My Dear Family and "My Dearest"

ACKNOWLEDGMENTS

I would like to thank to my supervisor Prof. Dr. Haluk Külah for his support, encouragement, and supervision throughout my study. I would also like to express my sincere gratitude to my co-advisor Assoc. Prof. Dr. Ender Yıldırım, for all his help and guidance throughout my studies.

I would like to express my thanks to Dr. Yağmur Demircan Yalçın for all her contributions to this study. I am deeply grateful to Dr. Özge Zorlu and Assoc. Prof. Ebru Özgür for their valuable remarks, opinions to motivations. I am particularly thankful to Taylan Töral and Ali Can Atik for carrying out microfabrication processes. I would like to thank to Şebnem Şahin and Gizem Karayalçın for carrying out blood processes for my experiments. Many thanks to Buket Şahin, for all her help to my experiments and thesis work. I am also thankful to Dr. Begüm Şen Doğan for her remarks and motivations throughout my work. I would also thank to all remaining Mikro Biyosistemler Family for making an enjoyable working environment.

I would like to thank to The Scientific and Technological Research Council of Turkey (TÜBİTAK) for supporting the project that this thesis is a part of. I would also like to thank to METU Medical Center for providing samples that are used in experiments.

Finally, I would like to express my deepest gratitude to my dear family; my dear mother, Nurten and my dear father, Rafi, for their support and love throughout my whole life. Lastly, I would like to thank to my dearest, Esra, for her unconditional love and support and always being there for me.

TABLE OF CONTENTS

LIST OF TABLES

TABLES

LIST OF FIGURES

FIGURES

CHAPTER 1

INTRODUCTION

Bacteria and viruses are main infections causing agents in human body. A clinician may identify the cause of an infection solely based on symptoms of the patient. However, this is not applicable for all cases. In some cases, to identify the infection causing agent's type extra blood work may be required.

Correct diagnosis of the infection type is critical in terms of managing the treatment. Most crucial aspect of managing the treatment against infections is determining whether antibiotic prescription is necessary or not. Antibiotics are agents that are used against bacterial infections [1]. Unnecessary or misuse of antibiotics is a major public health problem since they increase antibiotic resistance of the community [2]. Emergence of bacterium variants that is resistant to antibiotics is an issue associated with high morbidity and mortality [3]. Turkey is one of the countries which have the highest antibiotic consumption rates [4].So, managing antibiotic prescription is important especially in Turkey to fight against antibiotic resistance.

White blood cells (WBCs) are main infection fighting agents in human body. Their number increases in case of an infection in the body. However, increase pattern differs from infection to infection. White blood cells have two main subtypes that comprises most of them: Neutrophils and Lymphocytes [5]. Generally, in the case of an infection, if neutrophil ratio among all WBCs increases; this indicates a bacterial infection; however, if lymphocytes ratio among all WBCs increases this indicates a viral infection [6].

Differential count of WBCs is possible in today's technology. A standart hematology analyzer can provide these data. However, since they are expensive machines, hospitals have limited number of them. Some smaller hospitals or family health most of the time cannot afford to buy them. In addition, since these devices take up the

burden of whole hospital, obtaining results from them takes time. For these reasons, clinicians may tend to avoid ordering a complete blood count on a patient. There are different benchtop devices that provides differential WBC information however, since they are using optical detection techniques they are not cost efficient [7].

In the scope of thesis, a microfluidic device that utilizes impedance flow cytometry to obtain differential WBC count from a small amount blood is introduced.

1.1 White Blood Cells and Their Clinical Significance

White blood cells are the main infection fighting agents in the body. They are normally present in the blood, but their quantity increases during an infection in body [8]. They have two main subtypes called granulocytes and agranulocytes. Under these two subtypes, there are two cell types that comprises 85% of whole WBCs. These two cells are neutrophils and lymphocytes (Figure 1.1) [9]. Their total count and ratio to each other have many clinical applications ranging from cancer prognosis [10], cardiovascular diseases [11] to infections [12].

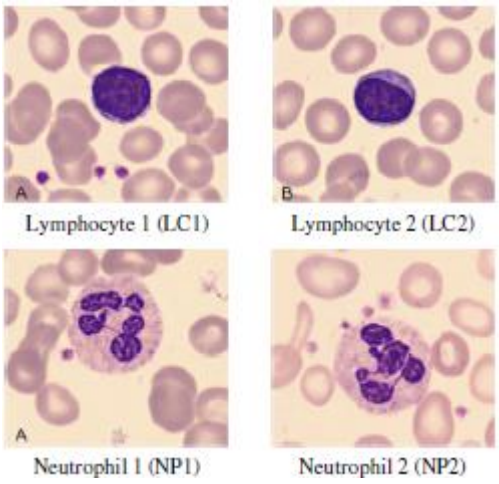

Figure 1.1 Microscopic Images of Lymphocyte and Neutrophils[13]

In the scope of this thesis their clinical significance in infections is discussed. As it is mentioned priorly, infections in humans mainly caused by two agents: viruses and

bacterium. Determination of origin of infection is important since this information mediates the treatment process.

Neutrophil to lymphocyte count ratio (NLCR) is an important clinical marker that is utilized in many clinical conditions [14]. Research show that elevated NLCR levels indicates a bacterial infection, since during a bacterial infection, neutrophil count increases whereas lymphocytes count decreases [15]. So, if an elevated NLCR is detected in a patient suffering from an infection, infection's origin at the patient can be correctly determined as bacterium. Then, clinician can mediate the treatment safely since origin of the infection is determined. On the contrary in the case of detection of normal or lower NLCR, infection origin can be determined as viral.

Lymphocytes and neutrophils have different sizes. Generally, lymphocytes are smaller than neutrophils. According to literature, average neutrophil size is between 10-12 μm and average lymphocyte size is between 6-9 μm [16].

1.2 Cell Counting Methods

There are different cell counting methods available. The first method is hematocytometer. Hematocytometer is standardized method. A standart hematocytometer chamber is given in Figure 1.2. A standart hematocytometer chamber contains larger and smaller square sections. Chamber restricts the area and the volume of the examined sample. Sample then examined under microscope. Since it's volume is known cell concentration can be achived at the end [17]. This method heavily depends on the operator, and sample needs to be preapared to make it suitable for examination. In addition, examining samples with larger concentrations is labor intensive. Also, differentiation of different cells is problematic since discrimination between different cell groups should be done by the operator [18].

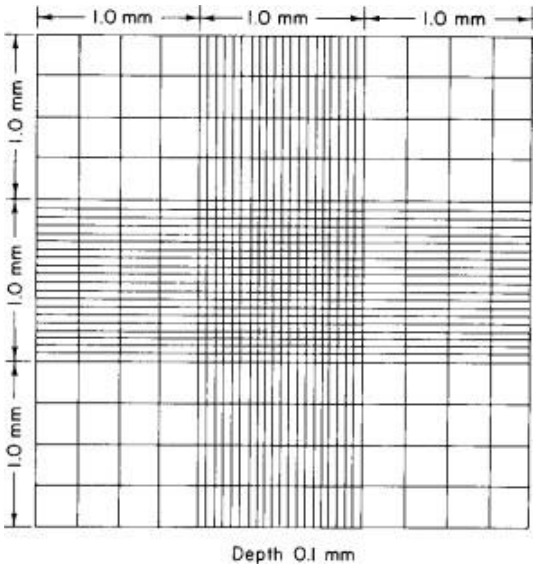

Figure 1.2 Hematocytometer

There are automated cell counters (Figure 1.3) that uses a similar method as hematocytometer. Difference between them is automated counting. Automated cell counters as in hematocytometer have chambers that can hold a known amount of sample. Using optical detection methods, they focus and count cells with image processing. They can provide histogram but cannot differentiate two different cell groups. Also, since they use very low amount of sample, there can be errors due to sampling in the cell count [19].

Figure 1.3 Automated Cell Counter [20]

Another method that is used for cell counting is flow cytometry. Flow cytometry devices can measure optical and fluorescence characteristics of cell and with these data they count and differentiate cells. Working principle of flow cytometry devices are as follows: A light from a source, generally a laser, is directed to a channel. Cells pass through that channel scatter the light and makes fluorescence emission. These optical data of cells are sensed by sensors and analyzed to count and differentiate cells [21]. Figure 1.4 illustrates the working principle of a flow cytometer.

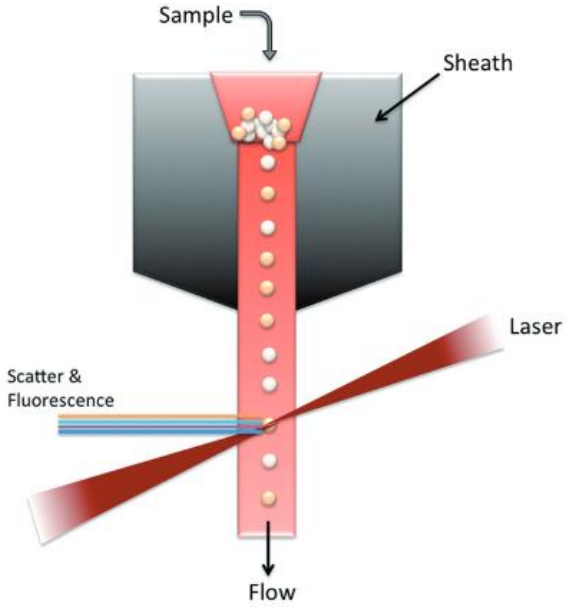

Figure 1.4 Flow Cytometry Working Principle [22]

Aside from these optical methods, there are methods that utilize impedance to count cells. These methods are investigated further.

1.2.1 Impedance Flow Cytometry

First cytometry device that uses electrical properties of the cell to characterize them is develop by Coulter [23]. The device utilizes a method for measuring the DC resistance between two fluid-filled chambers that are electrically isolated from one another, and for monitoring changes in this resistance as particles pass through a small connecting orifice. This measurement is achieved by positioning two large

electrodes at either side of the orifice, and utilizing the displacement of conductive fluid caused by the passage of a particle through the orifice to alter the resistance, which is then measured as a current pulse. Pulses count and amplitude corresponds to cell count and size respectively [24]. Figure 1.5 shows the opeation of Coulter counter.

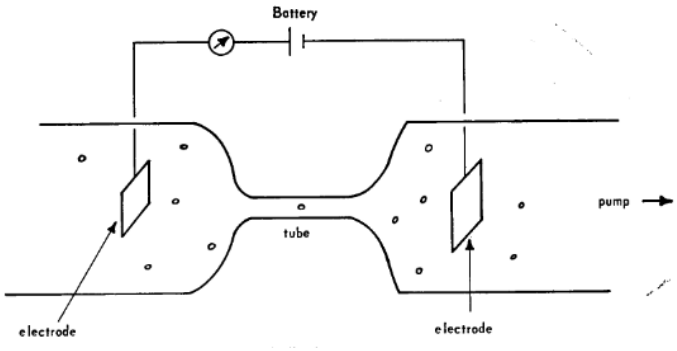

Figure 1.5 Coulter Counter Operation [25]

Over time Coulter counters miniaturized and become microfluidic impedance flow cytometers. There are different configurations of microfluidic impedance flow cytometer that are implemented in the literature. They differ in terms of their channel and electrode configurations. These electrode configurations, generally, can be breakdown into two main categories. These are coplanar and parallel facing electrode configurations [26] (Figure 1.6). In coplanar electrode configuration, electrodes lie at the same surface on the microchannel. In the parallel facing electrode configuration, as the name implies, electrodes lie on the opposite sides of the microchannel, facing each other.

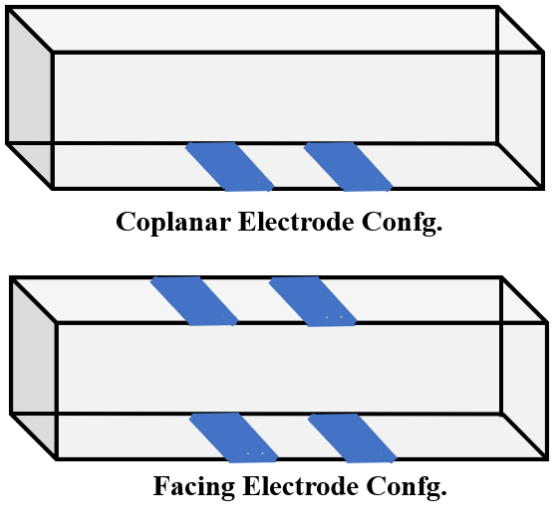

Figure 1.6 Two Main Electrode Configurations in IFC

In 2001, Renaud and colleagues [27] were the first to introduce the use of microfluidics in impedance flow cytometry, a technique for high-throughput characterization of the electrical properties of individual cells. They utilized a chip with integrated channels and a differential pair of coplanar microelectrodes to measure impedance data at two specific frequencies as cells were rapidly passed through the measurement area. The microfluidic device was employed to showcase its capabilities by differentiating between latex beads of 5 and 8 μm in size. The outcome verified that the impedance data collected at low frequencies accurately reflects the sizes of the particles. Additionally, the device was utilized to distinguish between normal erythrocytes and erythrocyte ghost cells, which are erythrocytes with the cytoplasm replaced by phosphate buffer solution at higher frequencies.

In 2005, Renaud et al. [28] suggested a new configuration for microfluidic impedance flow cytometry, which employed parallel overlap microelectrodes in place of the previously used coplanar microelectrodes, thus allowing for the production of a more uniform current density around the individual cells under examination. Experiments were conducted to classify polystyrene beads of 5 and 6 μm, normal red blood cells, and fixed red blood cells based on the impedance data obtained at low and high frequencies.

1.3 Research Objectives and Thesis Organization

Fast detection of infection type is important in clinical applications since it determines the clinician prescription to patient. Especially, prescription of antibiotics without a certain diagnosis contains risks. Unnecessary consumption of antibiotics has potential to increase antibiotic resistance of bacterium. Therefore, ensuring infection type of the patient before deciding on the treatment is critical for the clinician.

For these reasons a microfluidic impedance flow cytometry device that aims provide neutrophil – lymphocyte differential count is decided to be developed. This thesis focuses on main diagnosis unit of this device, a microfluidic impedance flow cytometry chip and its cartridge.

Main research objective of this thesis is to develop and validate a microfluidic impedance flow cytometry device that can enumerate and differentiate two different cell groups that passes through it, and implementation of it with a chip cartridge to make it usable with a microfluidic platform with ease.

To achieve this objective following tasks are carried out:

- Design and implementation of a microfluidic impedance flow cytometry device.
- Validation of performance of the impedance flow cytometry device with microbeads and cells of interest.
- Implementation of impedance flow cytometry device with a chip cartridge.

In chapter 2 theoretical background of the used method is given among with detection principle of the device. Chapter 3 includes device design, simulation, fabrication process and also explains experimental processes. In chapter 4 experiment results are given and discussed. Finally, chapter 5 concludes the thesis and present possible approaches for future work.

CHAPTER 2

THEORETICAL BACKGROUND

This chapter summarizes used technique for development of the device that is in the scope of this thesis work.

2.1 Impedance Flow Cytometry Theory

In impedance sensing, a signal that varies in frequency is applied to the system and the response is measured. Typically, a small AC voltage signal (usually sinusoidal) is used as the excitation and the electrical current response is measured. The complex impedance (Z(ω)) of the system can then be calculated by using the ratio of the excitation signal (U(ω)) to the response signal (I(ω)) [29].

$$Z(\omega) = \frac{U(\omega)}{I(\omega)} = Z_{RE} + jZ_{IM} \quad (2.1)$$

The complex impedance can be broken down into two parts: the real part, known as resistance, and the imaginary part, known as reactance. The magnitude and phase angle of the complex impedance can also be calculated, with j being equal to -1 and ω representing the frequency, as follows:

$$|Z| = \sqrt{(Z_{RE})^2 + (Z_{IM})^2} \quad (2.2)$$

Theoretical model used in impedance-based techniques is the electrical model of a single cell in an aqueous medium. A widely accepted model for electrical properties of biological cells with a lipid bilayer plasma membrane is the "single-shell" model (Figure 2.1). This model consists of a conducting sphere (representing the cytoplasm as a homogeneous phase) and an insulating thin shell (representing the plasma membrane) [30]. The equivalent complex permittivity of this mixture can be described by the well-known Maxwell's mixture theory [31]:

$$\varepsilon_{mix} = \varepsilon_m \frac{1+2\varphi f_{CM}}{1-\varphi f_{CM}} \quad (2.3)$$

In the equation, the complex permittivity of the medium-cell mixture, suspending medium, and cell are represented by ε_{mix}, ε_m, and ε_c, respectively. The volume fraction of the cell to the detection area is represented by φ, and the complex Clausius-Mossotti factor is represented by f_{CM}.

$$f_{CM} = \frac{\varepsilon_c - \varepsilon_m}{\varepsilon_c + 2\varepsilon_m} \quad (2.4)$$

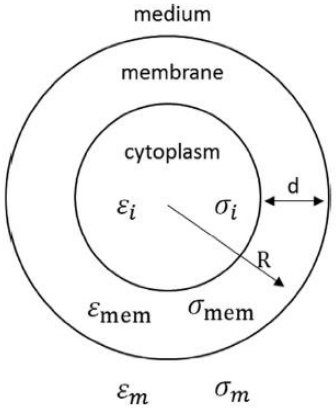

Figure 2.1 Single-shell model of a single cell in suspension [30]

For a single-shelled spherical cell model, ε_c is:

$$\varepsilon_c = \varepsilon_{mem} \frac{\rho^3 + 2\left(\frac{\varepsilon_i - \varepsilon_m}{\varepsilon_i + 2\varepsilon_m}\right)}{\rho^3 - \left(\frac{\varepsilon_i - \varepsilon_m}{\varepsilon_i + 2\varepsilon_m}\right)} \quad (2.5)$$

$$\rho = \frac{R}{R-d} \quad (2.6)$$

Where permittivity of the medium, cell membrane, and cytoplasm are represented by ε_m, ε_{mem}, and ε_i respectively, while the conductivity of the medium, cell membrane, and cytoplasm are represented by σ_m, σ_{mem}, and σ_i respectively. The radius of the cell and the thickness of the membrane are represented by R and d respectively.

The complex impedance of the cell-medium system, Zmix, is then represented by:

$$Z_{mix} = \frac{1}{j\omega C_{mix}} \quad (2.7)$$

The complex capacitance of the system, C_{mix}, is determined by the value of ε_{mix} and is reflected in the equation for Z_{mix}.

$$C_{mix} = \varepsilon_{mix} \frac{S}{4\pi kd} \quad (2.8)$$

Moreover, to the information provided priori, Koch et al. states that the equation for calculating the change in impedance (ΔR) in a classical Coulter counter when a spherical particle of radius (r_p) is present is:

$$\Delta R = 2\rho_{sol}\left[\frac{\operatorname{atan}\left(\frac{r_p}{\sqrt{\frac{A_C}{\pi}-r_p^2}}\right)}{\pi\sqrt{\frac{A_C}{\pi}-r_p^2}} - \frac{r_p}{A_C}\right] \quad (2.9)$$

2.2 Electrical Cell Detection

An electrical circuit analogy is commonly employed to simplify the analysis of a system, and this approach was established by Foster and Schwan in 1989 [32]. The cell is represented as a resistor that represents the cytoplasm in combination with a capacitor for the membrane, as illustrated in Figure 2.2. Other than that, there are cell models that is called double shell cell models. In double shell models, effect of cell nucleus and nucleus membrane is also considered [33]. In this study single shell model is utilized for simplicity.

The cell membrane resistance is typically much greater than the reactance of the membrane and is typically disregarded. Similarly, the capacitance of the cell cytoplasm can be disregarded when its reactance is compared to the cell cytoplasm resistance.

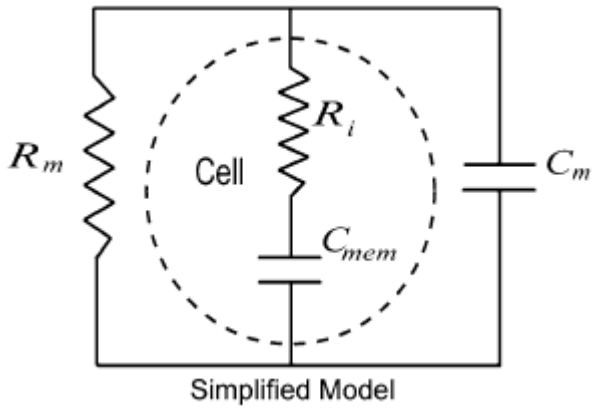

Figure 2.2 Simplified Circuit Model for a Single-Shell Cell in Suspension [34]

The values of electrical components in the simplified model as follows:

$$R_m = \frac{1}{\sigma_m\left(1-\frac{3\varphi}{2}\right)lk} \quad (2.10)$$

Where volume fraction φ:

$$\varphi = \frac{4}{3}\pi R^3 \frac{1}{k\omega lh} \quad (2.11)$$

l in the equation 2.11 corresponds to electrode length. k is the cell constant; it is equal to w/h when electric field is homogenous where w and h are electrode width and channel height respectively.

$$C_{mem} = \varepsilon_\infty lk \quad (2.12)$$

$$C_{mem} = \frac{9\varphi R C_{mem,O}}{4} kl \quad (2.13)$$

$$R_i = \frac{4\left(\frac{1}{2\sigma_m}+\frac{1}{\sigma_i}\right)}{9\varphi kl} \quad (2.14)$$

$$C_{mem,O} = \frac{\varepsilon_m}{d} \quad (2.15)$$

$C_{mem,0}$ represent the specific membrane capacitance and permittivity at infinite frequency represented by ε_∞. So, total impedance can be determined by utilizing the formula:

$$Z_{mix} = \frac{R_m(1+j\omega R_i C_{mem})}{j\omega R_m C_{mem}+(1+j\omega R_i C_{mem})(1+j\omega R_m C_m)} \quad (2.16)$$

If a differential measurement is utilized in the system, then impedance peak value would be:

$$\Delta Z = Z_{mix\_DL} - Z_{m\_DL} \quad (2.17)$$

Figure 2.3 shows a coplanar electrode configuration with differential measurement, represented by its circuit equivalent.

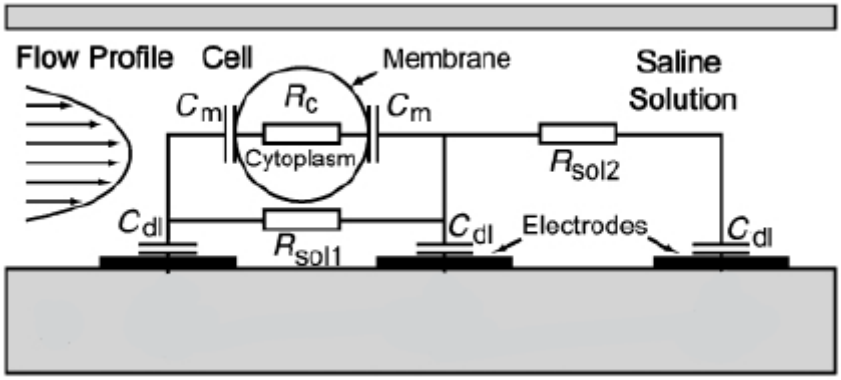

Figure 2.3 Coplanar Electrode Configuration with Differential Measurement Electrical Equivalent [27]

CHAPTER 3

MATERIALS AND METHOD

This chapter explains used methods regarding the design and simulation of the devices that are used in the scope of thesis work, used devices fabrication process and experimental work that has been done for the tests of the devices.

3.1 Microfluidic Device Design

Different design alternatives that can be utilized for IFC applications are given in section 1.2. Among these designs, coplanar electrode formation with three electrodes is choosen as the final electrode formation of the device that is to be fabricated. Microchannel is decided to be straight rectangular channel also. Main reason of this selection is ease of fabrication and references that present good results with similar electrode configuration. Since this thesis work is a part of a BioMEMS Research Group project, initial design and fabrication of the IFC devices were already completed when this thesis work had started. Device parameters are selected based on the designs that are implemented on the literature [26], [27], [35]–[38]. There are mainly four design parameters: Channel depth (z), channel width (y), electrode width (w) and electrode spacing (s). Design parameters are shown in a simple channel in Figure 3.1.

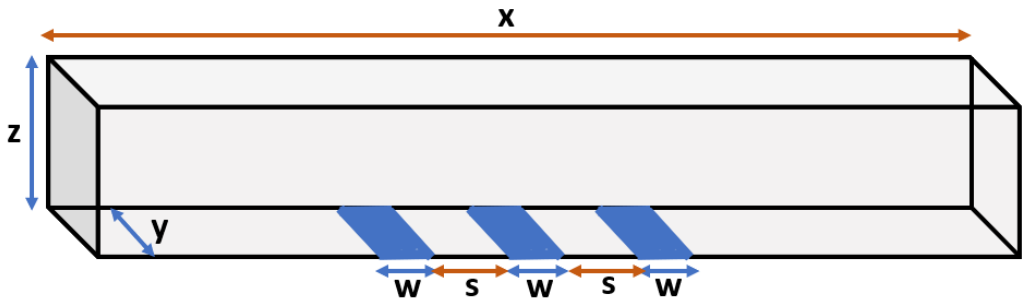

Figure 3.1 Design Parameters of IFC Device

Three design is proposed and fabricated. Their specifications are provided in Table 3.1. At proposed designs, channel width and depth selected as 30 µm for all designs. Also, channel length is same with 2000 µm. Only thing that differs between designs are electrode widths, since electrode spacings are also same with 20 µm. Electrode widths are 14, 20 and 30 µm for Type 1-2 and 3 designs respectively.

Table 3.1 Designed Microchannel and Electrode Properties

Design Code	Channel Width (y) (µm)	Electrode Width (w) (µm)	Electrode Spacing (s) (µm)
Type 1	30	14	20
Type 2	30	20	20
Type 3	30	30	20

Layout images of the IFC device design on die level is given in Figure 3.2. A widening channel is implemented at the beginning and ending of the microchannel due to port size limitations. Electrodes are lying in cavity along the chip to prevent contact with silicon layer of the device. Three microchannel and two electrode structures are included into a die due to availability of space on a die.

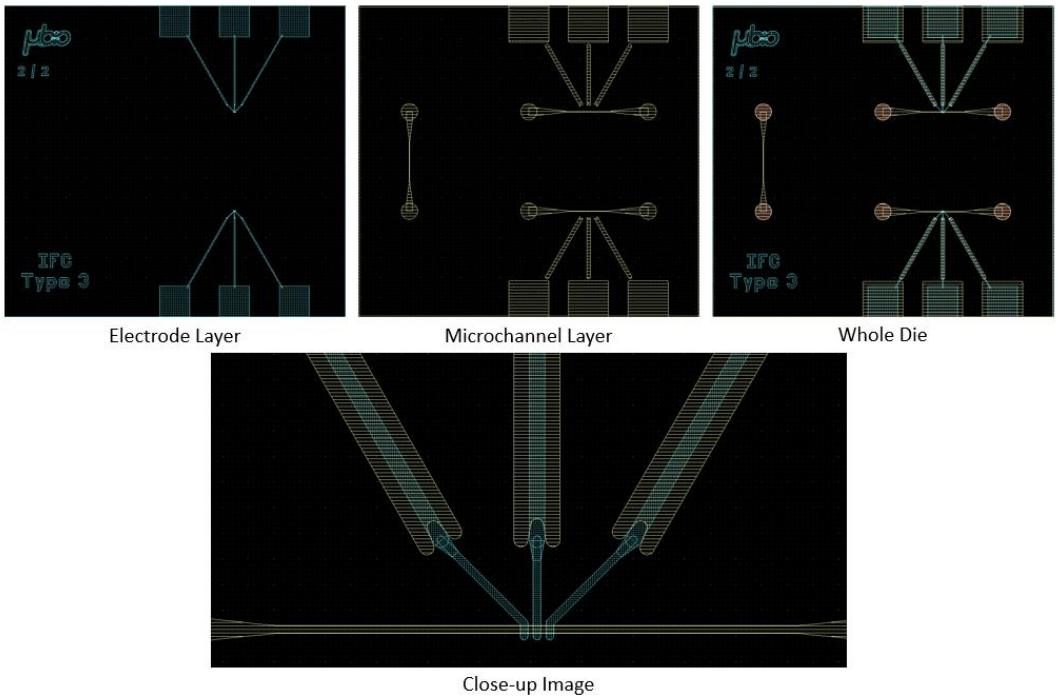

Figure 3.2 Layout Images of IFC Device Design

3.2 Device Parameters Simulation

Current Design Validation Simulations

Device parameters are decided to be simulated around the existing design parameters to check if there is a need for a new design and fabrication. For this purpose, selected parameters of the device need to be determined if they are appropriate for detection of cells of interest, lymphocytes, and neutrophils. Main parameters of the device are determined as electrode width, electrode spacing and channel height. Channel width also corresponds to electrode width is determined to be selected and remain constant throughout the simulation among with channel length since they are not significant for cell detection [39]. Reason of this is the cell flow direction in the device. As cells flow through the length of the channel only region that have significance in terms of electrical detection are around electrodes that lies below the channel. So, channel length is not expected to affect the measurement that is to be taken with the help of electrodes as long as three electrodes have enough space to lie below the channel.

Another parameter that is determined to have no significant effect in electrical measurement of cells is y position of the cell which corresponds to electrode length in y direction. As cells flow through the channel no matter the y position in the space, they will go through same electrical field lines [40].

To show the change of the impedance through the microchannel as micro-beads or cells pass, a simulation model was necessary. COMSOL Multiphysics software AC/DC module was the platform that is chosen for these simulations. A straight rectangular channel geometry is decided to be used. Initially, deviation of electrical response based on channel's geometry change is determined to be examined. For this purpose, main channel geometry properties are decided as channel height, width, electrode width and electrode spacing. Since fluid flow simulation is not planned to be done at this stage, channel length of the model solely decided on electrical response. Channel length is determined at a level such that electrical response acquired at electrodes while micro-beads or cells at the beginning or the end of the channel is almost equal to zero. By doing this one can decide between different geometries according to their electrical response, knowing that electrical response acquired at simulation is only because of selected parameters. Also, channel length tried to be as low as possible while satisfying the aforementioned property so that simulation duration would be lower since electrical response from electrodes at simulation is calculated at each position in channel space with an interval.

Simulation calculates the current formed at two outer electrodes that is defined at the geometry. Middle electrode is used to create the electrical field in the micro channel. Middle electrode electrical voltage value set to 1V at the simulation. This voltage as it is mentioned creates an electrical field inside the micro channel. Micro channel's all surfaces are defined as insulator except electrodes. Microbead and its position is defined mathematically as a sphere (3.1).

$$R_{sq} = ((x - x_0)^2 + (y - y_0)^2 + (z - z_0)^2) \quad (3.1)$$

Fluid that should be present at micro channel is PBS, so necessary parameters of PBS for the simulation are entered. PBS conductivity (sig_bulk) and relative

permittivity (eps_r_buk) set as 1.6 S/m and 78 respectively [41]. Particle that should flow in the micro channel is decided to be modeled as a micro bead. As PBS, micro bead is also modeled mathematically. Micro bead is modeled as an insulator since they are polystyrene solid particles. So, its electrical conductivity and relative permittivity is entered as 0 and 1 respectively.

Material conductivity defined as:

$$\text{sig\_bulk} * (\text{Rsq} > r_0{}^2) \qquad (3.2)$$

which is equal to PBS conductivity outside the sphere, zero inside the sphere.

Material relative permittivity defined as:

$$1 + (\text{eps\_r\_bulk} - 1) * (R_{sq} > \text{r}_0{}^2) \qquad (3.3)$$

which is equal to PBS relative permittivity outside sphere, 1 inside the sphere.

A steady state time independent simulation is carried out. Micro beads are positioned at different points in the channel space and their electrical response is calculated. COMSOL Model geometry that is used given in Figure 3.3.

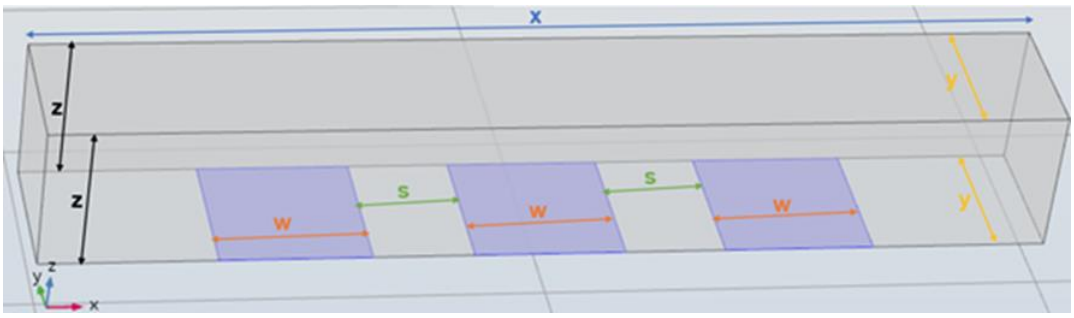

Figure 3.3. COMSOL Model Geometry and Parameters

First simulation is aimed to be done in order to determine the particle positions that should be included in the actual simulations. Simulating the particles at each position in micro channel space is an option, however, this would take so much time since simulation calculates the electrical response at each position one by one. If simulating some positions in the space is rudimentary then omitting these positions from the simulation would decrease the simulation time. So, in order to determine

the necessary positions to be simulated, electrical response at each two-dimensional pairs will be simulated. By examining the results of these dimensional pair simulations, an unnecessary dimension, if there is any, can be determined. Following simulation is conducted with 6µm and 10µm diameter beads. YZ and Z sweeps results that is performed for this purpose are given in Figure 3.4. and 3.5

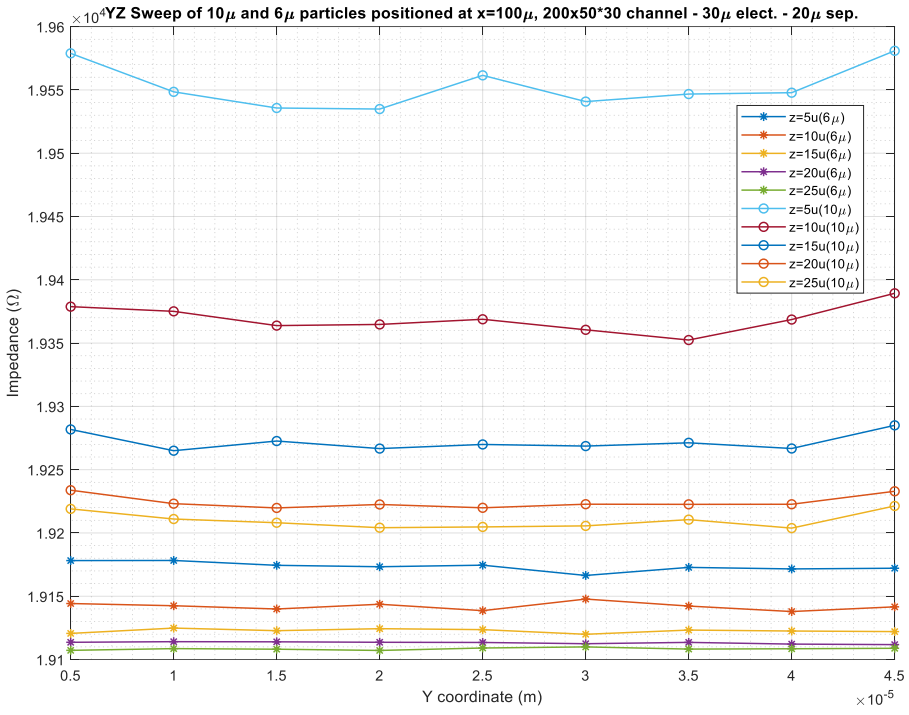

Figure 3.4 6-10µm Bead YZ Sweep, X Constant, Simulation Results

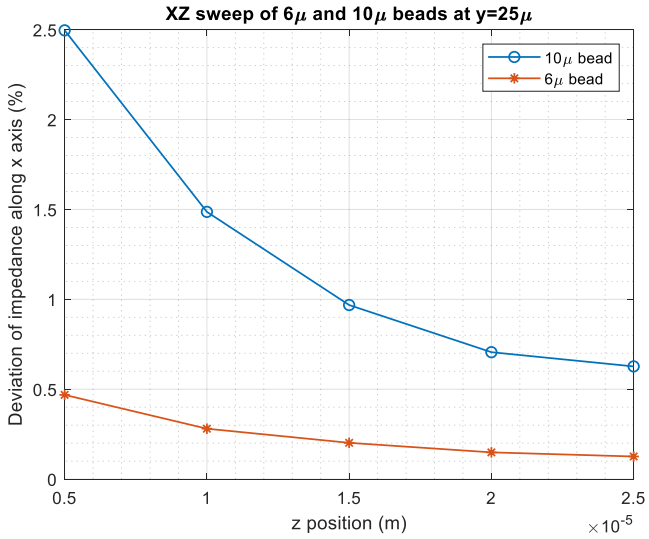

Figure 3.5 6-10um Bead Z Sweep, XY Constant, Simulation Results

If simulation results in Figure 3.4 are examined it can be seen that changing the position at y axis while x and z positions are constant, changes electrical response at a negligible rate. However, as it can be seen from Figure 3.5, changes in z positions while the other two stay the same, changes the simulation results considerably. This outcome was expected as this way since in the literature there are publications that has shown this phenomenon [39]. In the light of these results simulations are decided to be conducted while micro beads' positions move along the xz plane and y position of the micro bead is constant at the center of the y axis of the micro channel.

Since the simulation sweep dimensions are identified, numerical values for micro channel geometry should be defined. Starting point is chosen as existing Type 3 design. Then by putting this starting point to the center, different geometry parameters are decided to be simulated to find an optimum point for differentiating 6µm and 8µm micro particles. 6µm and 8µm diameter values are determined experimentally by using a cell counter device to measure lymphocytes and neutrophils. Lymphocytes and neutrophils average diameters are determined from histograms that cell counter device provides.

Selected reference geometry parameters are given in Table 3.2. Three coplanar electrode structure is implemented as design. Middle electrode is used as an excitation electrode, whereas side electrodes are utilized as sensory electrodes.

Table 3.2 Reference Geometry Parameters

Channel Height (z)	Channel Width (y)	Electrode Width (w)	Electrode Spacing (s)
30 µm	30 µm	30 µm	20 µm

Excitation electrode is assigned to 1V voltage value. This voltage creates an electric field inside the micro channel. Deviation of this electric field creates a current response at measurement electrodes. Simulation model gives these current values at measurement electrodes. Difference between these currents taken as the electrical response of this system to simulate differential impedance measurement that is aimed to be implied practically in later stages.

Channel length is not significant in this simulation since particle flow is not simulated with a fluid flow simulation. Particles placed on different positions in space in micro channel in a time independent simulation. So micro channel length is determined so that when micro particles are stationed at the beginning and end of the channel, current reading obtained from the simulation is either zero or close to zero. This ensures when a micro particle is at the beginning or end of the channel, there is no effect of it observed electrically [42].

Initially it is thought to be more beneficial to simulate geometries with parameters at reasonable maximum and minimum values to get a better picture of the effect of determined parameters' variations. So, in order to accomplish that, the first set of parameters that is to be simulated is given in Table 3.3. Previous simulation results showed that change in y position does not change the electrical response so channel width (y) is kept as the reference geometry. Channel length (x) as it mentioned before is adjusted according to total length of electrodes and spacings in order to get close

to zero current response at the edges of the channels. Channel length tried to be kept as short as possible by keeping the condition in the mind to reduce the simulation time.

Table 3.3 Simulated Model List 1

Model No.	x (µm)	y (µm)	z (µm)	w (µm)	s (µm)
1	100	30	20	10	5
2	100	30	40	10	5
3	200	30	20	10	50
4	200	30	40	10	50
5	200	30	20	30	5
6	200	30	40	30	5
7	250	30	20	30	50
8	250	30	40	30	50

An example simulation result is given in Figure 3.6. Plot is obtained such a way that it demonstrates the bead flow from beginning to end of the channel. Different colored lines shows different z positions where bead travels through the channel. As expected, impedance obtained was maximum at lowest z position and lowest at highest z position. Also, again as expected, 8µm bead showed a greater impedance response than 6µm bead.

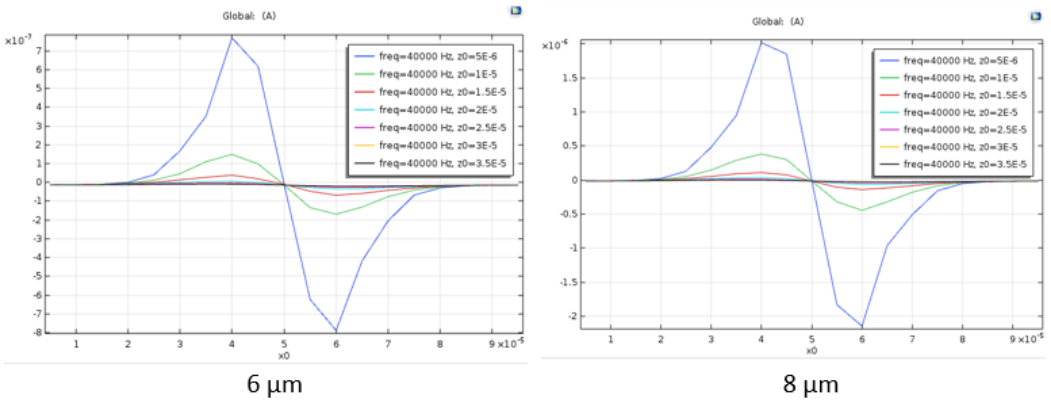

Figure 3.6 An Example Simulation Result

Main aim in this thesis is differentiating 6 and 8µm cells. So, if different size beads' impedance interval along z position does not coincide with each other, a differentiation can be obtained certainly. To check if that situation is achieved or not a new parameter is identified. That parameter is 8min – 6max. 8min is the minimum impedance of 8µm bead at different z positions and 6max is the maximum impedance of 6µm bead at different z positions. If this parameter is above zero and maximized, a differentiation among beads can be achieved at all conditions regardless the z position.

To check what channel, electrode parameter effects 8min-6max parameter more significantly a regression equation obtained for 6um and 8um particles. Difference between maximum impedance response of 6um particle and minimum impedance response of 8um particle is used as a solution for regression and a linear fit is attempted with respect to z, w and s (elec. spacing) parameters. Obtained regression equations and R-sq values are provided in Appendix A1:

Main effects plot for the fit is obtained to determine the weights of z, w and s parameters in the regression equation. Main effect plot shows the desired parameters change between simulated parameters minimum and maximum values. So, a steeper line means more effect on the desired parameter. If parameters that have more effect on the 8min-6max can be identified, further values of this parameters can be

simulated to cover more possibilities. Created main effect plot for this purpose is given in Figure 3.7.

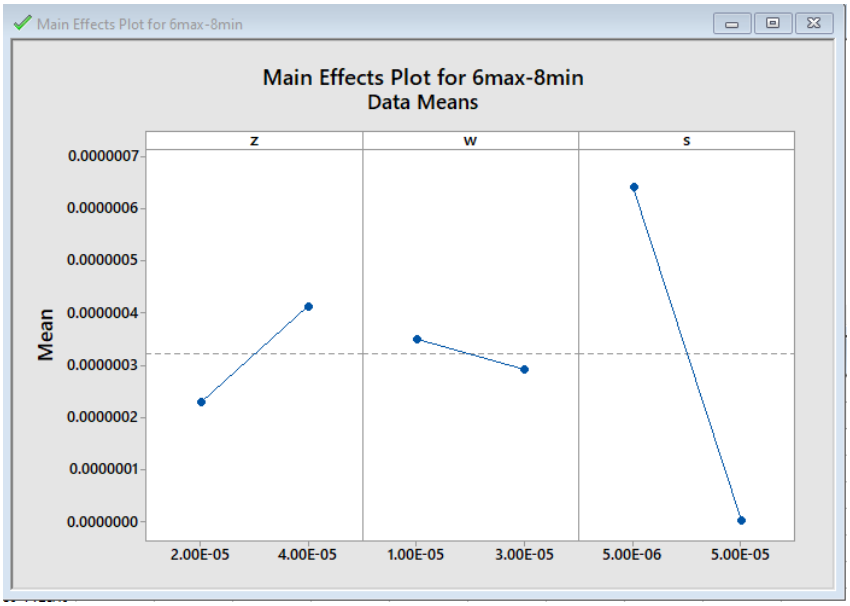

Figure 3.7 Main Effects Plot for 6max-8min

As it can be seen from the plot, most important parameter appeared to be s. And also, w parameter seems to have very low effect compared to others. So, for further simulations w is determined to be fixed at 30um (Type 3 design spec.). Apart from that, z parameter has physical constraints, so it is also fixed at 30um (Type 3 design spec.). Because further decreasing the z dimension would make the microchannel very prone to clogging during experiments. According to these factors new geometries that is decided to be simulated given in Table 3.4.

Table 3.4 Simulated Model List - 2

Model No.	x (µm)	y (µm)	z (µm)	w (µm)	s (µm)
9	200	30	30	30	5
10	200	30	30	30	10
11	200	30	30	30	20
12	250	30	30	30	30
13	250	30	30	30	40
14	250	30	30	30	50

Another parameter is determined for analysis of simulation results of this models. That parameter is 8mid-6mid. 8mid and 6mid is the impedance response of 8 and 6µm when they are at the center of the channel on z plane. It is identified to help to determine the design that distinguishes these two beads best when particles flow at the middle of channel height. When this value is maximum as in 8min-6max, it means that best distinction among these two beads is achieved. Regression equations with different terms for these parameters are obtained using all simulation results. Obtained regression equations and Rsq values are provided in Appendix A2.

Contour plots for these equations are obtained. Max values for both parameters are desired operating points. Plots are given in Figure 3.8.

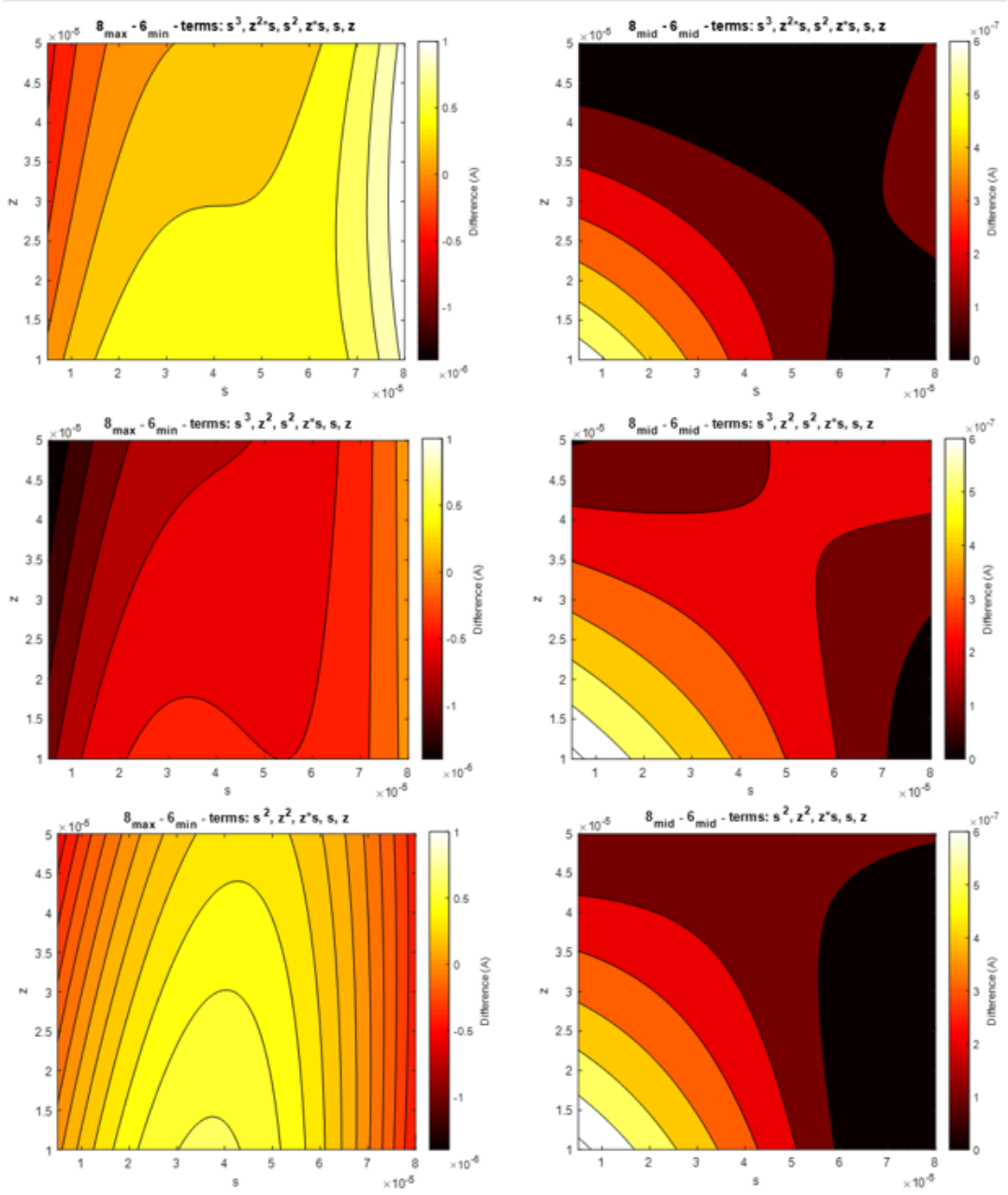

Figure 3.8 Contour Plots Obtained for Different Regression Equations

When these plots are analyzed it is decided that the geometry which have z=45µm, w=30µm and s=80µm dimension may work better than the current design in terms of distinguishing these two beads.

Simulation of the channel that is determined based on contour plots is performed. Fig 1. shows the xz sweep simulation results. Results are showed in the table. Current

design (Type 3 - z30um, w30um, s20um) results are also included in the table for comparison. All currents that are showed in the table are deviations from the baseline current that appears at x=0 position of channels. Simulation results and values obtained for that operation point from contour plots are included in the table to check validity of regression equations with simulations.

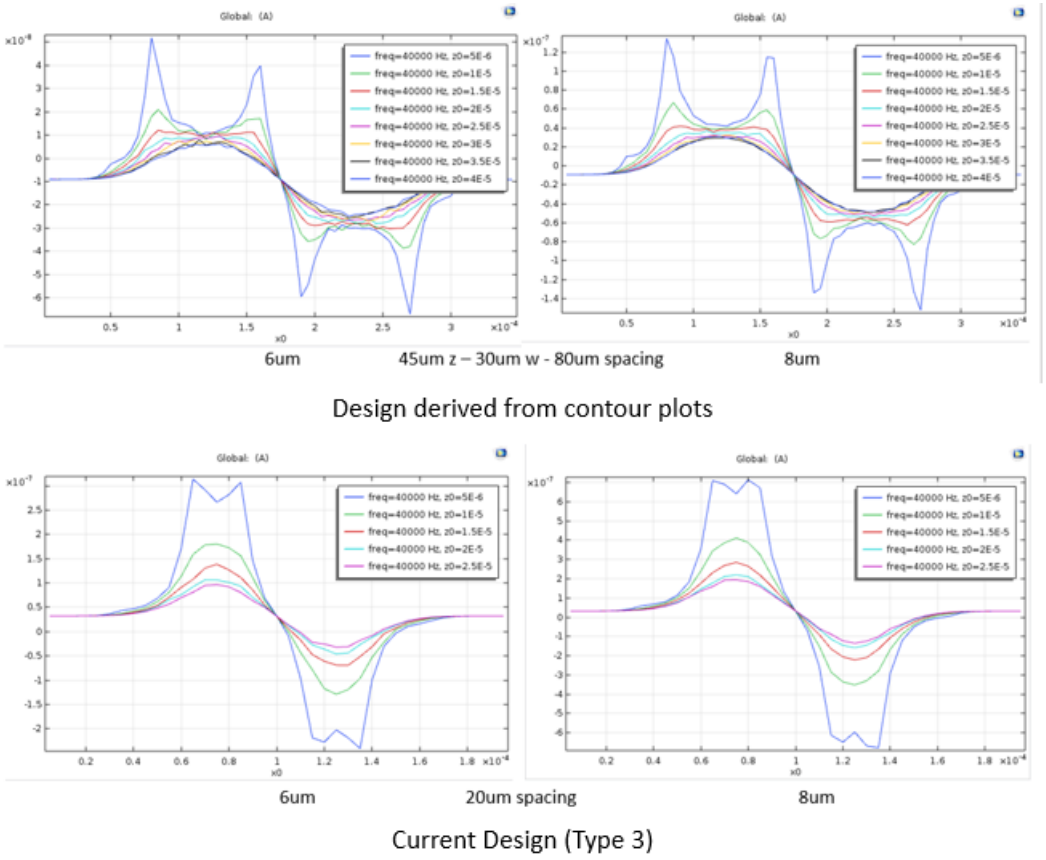

Figure 3.9 Comparison of Derived and Current Design

Table 3.5 Simulation Results and Estimated Values in Contour Plots (Bolds indicate closest estimated values to simulations)

	8min-6max	8mid-6mid
Type3 (Simulation)	-1,20E-07	1,46E-07
Type3 s3_z2s_s2	**4.635E-08**	-6.344E-08
Type3 s3_z2_s2	2.325E-07	**1.873E-07**
Type3 s2_z2	**3.556E-08**	**1.804E-07**
Type3 z3_s3_zs2_z2s	-3.438E-07	-2.519E-07
Opt. Des. (z45_w30_s80) (Simulation)	-2,24E-08	2,26E-08
Opt. Des. s3_z2s_s2	1.737E-07	-1.881E-07
Opt. Des. s3_z2_s2	3.567E-07	**6.299E-08**
Opt. Des. s2_z2	1.900E-07	**5.424E-08**
Opt. Des. z3_s3_zs2_z2s	**-2.092E-07**	-3.712E-07

At proposed optimum design parameters, acquired currents are decreased around 10 times for each case compared to current Type 3 design. Current detection problem may occur in the real application.

At proposed optimum design 8min-6max current value is not positive as expected from regression equations. Also, 8mid-6mid value is very small which may be a problem in distinction between two particles since that small current deviation may not be detected correctly at all times since it can disappear in the noise from the impedance spectroscope.

So, in the light of these information contour plots are examined again. Examination of these plots reveal that current type 3 design in fact very close to the optimum practical design that can be implemented. So, to avoid new mask expenditure, it is decided to carry on the experiments with current design.

PDMS-Glass Alignment Simulations

PDMS-Glass devices' bonding is going to be made by an operator without usage of any alignment tool. This can cause some alignment problems between channel and electrode structures. That is to say, electrodes can lie below the channel with an angle. To check if this may cause a significant problem in the measurements, it is decided to simulate misaligned electrode-microchannel geometries. An example misaligned model is given in Figure 3.10.

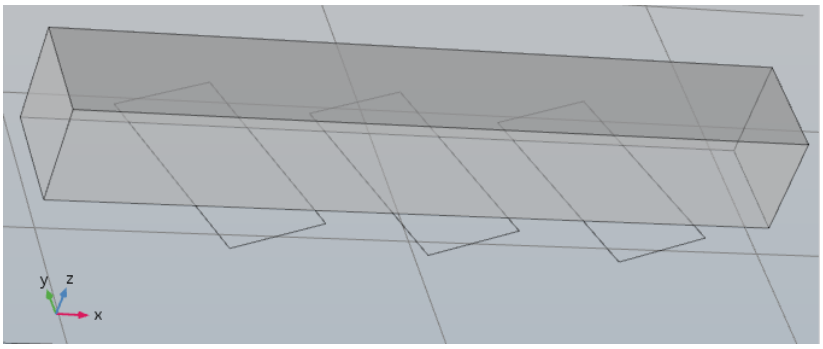

Figure 3.10 Example 20 Degree Misaligned Geometry

30um width electrodes with 20um spacings is used. Channel with 30um height is used. Sweep results obtained for 0-5-10-20-30 degree misalignments are obtained. XY, YZ and XZ sweeps are obtained. Results are provided in Figure 3.11.

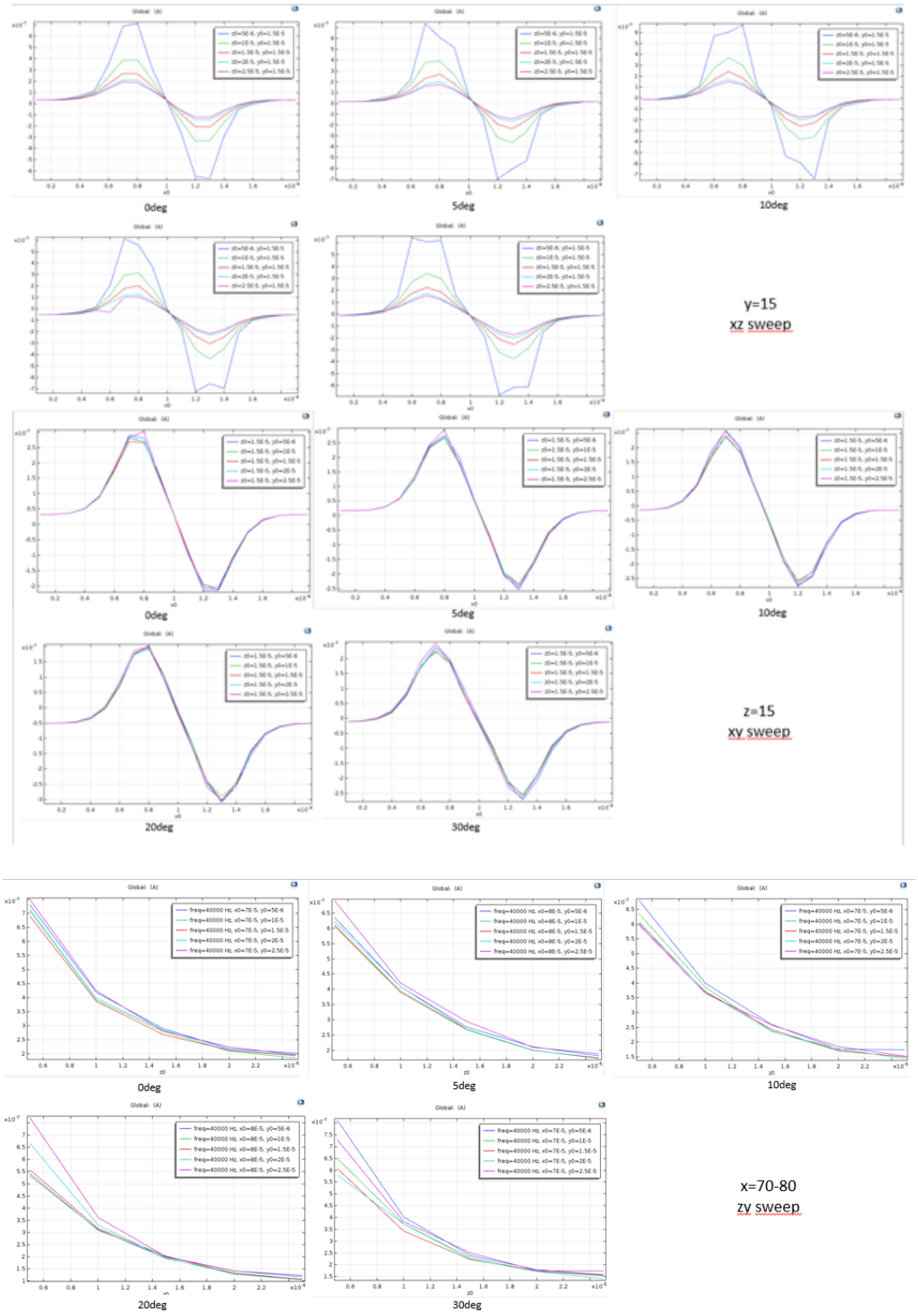

Figure 3.11 Misaligned Geometries Sweep Results

If one examines the plots that are obtained after simulations, it can be seen that misalignment does not create a significant deviation at the impedance that is obtained from the channel.

3.3 Microfluidic Device Fabrication

For fabricating designed device two fabrication methods are decided to be implemented. Those two methods are Si-Glass and PDMS-Glass. Si-Glass MEMS fabrication is implemented since it is a stable and well-known process inside our research group. Also, PDMS-Glass fabrication is decided to be implemented because regardless the oxide layer between them, there was a doubt that electrodes can be affected by the silicon layer since it is a semiconductor. To make sure that electrodes do not affect by any conductive surface, PDMS-Glass fabrication is ideal since PDMS is an insulator. Also, another advantage that PDMS-Glass fabrication may be the sealing between two layers. Since PDMS is a soft material, when it is bonded with a hard material it can act as a gasket and can provide a better seal for fluid leakage. Si-Glass chips and PDMS mold fabrications are carried out by METU MEMS Center personnel.

3.3.1 Si-Glass Device Fabrication

The microfluidic chips were fabricated with a MEMS-based silicon glass stack process where the microfluidic channels were formed at the silicon side. In this fabrication method, microchannels are formed on silicon wafers and metal electrodes are formed on glass wafers. These silicon and glass wafers are then bonded together. The fabrication method starts with a pre-cleaning process (Step 1). Next, the channels on the silicon active surface are shaped by photolithography (Step 2) and the desired channel depth is formed by DRIE (Deep Reactive-Ion Etching) etching (Step 3). Then, photoresist and DRIE polymer residues are removed by oxygen plasma etching (Step 4). After this step, the channels pattern is formed on the active

surface of the silicon wafer. In the next step, the microfluidic inlet and outlet ports were then formed with a second DRIE process, which is now applied from the backside of the wafer along its thickness by using the thermally deposited SiO2 as a masking layer as well as the photoresist used for patterning the SiO2 (Step 7). Next, the oxide layer on the back surface is etched with BHF (buffered hydrofluoric acid) using the photoresist mask (Step 8). Then, under the cover of both oxide and photoresist layers, the silicon wafer is etched by DRIE until it reaches the front surface (Step 9). After this step, cleaning processes are applied on the silicon wafers (Step 10). The oxide layer is finally removed by BHF etching (Step 11). Finally, the silicon wafers are coated with thermal silicon dioxide for surface insulation and the same anodic bonding process, again following RCA and DHF (diluted HF) pre-oven cleaning (Step 14). In parallel, BF33 borosilicate glass wafers are pre-cleaned with piranha (Step 16). In the next step, the glass wafers are masked with photoresist to create the cavities in which the electrodes will be embedded in the glass using the BHF wet etching method (Step 17). In this way, the photoresist mask can be used for both the opening of the BHF cavity and the removal of the metal by lift-off. Ti/Pt metal electrodes are coated in the BHF cavities at a level 10 nm below the glass surface level and the metal electrodes are shaped by lift-off (Step 18). In the next step, the silicon and glass wafers are aligned and bonded together by anodic bonding after a short piranha activation process (Step 19). Thus, the designed microfluidic

channels are prepared. Finally, the bonded silicon-glass wafers are diced of the intended size and the fabrication process is completed.

Process flow is provided in Figure 3.12.

SEM image of silicon wafer and finished device's image under microscope is given in Figure 3.13-14.

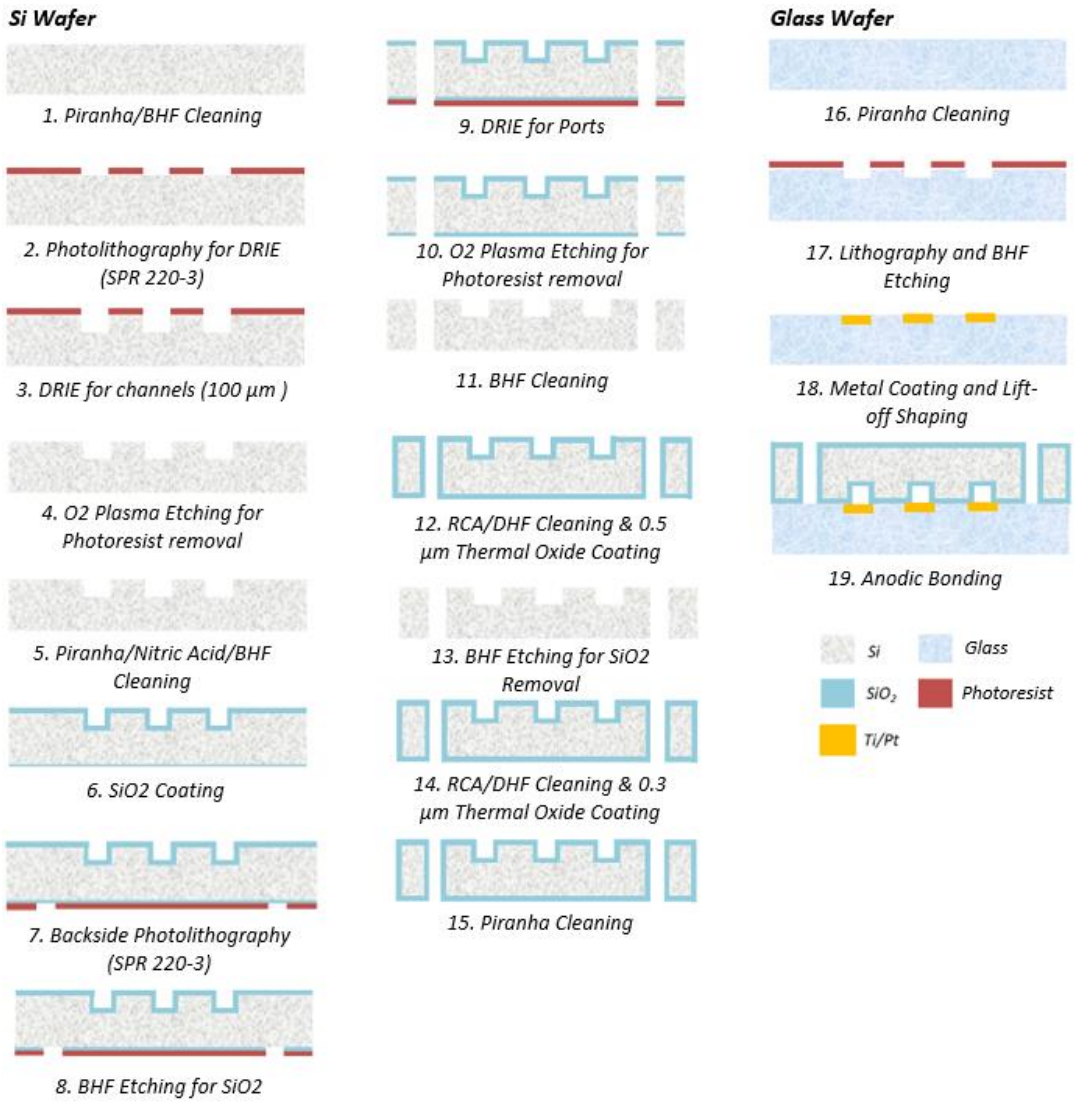

Figure 3.12 Si-Glass Device Fabrication Steps

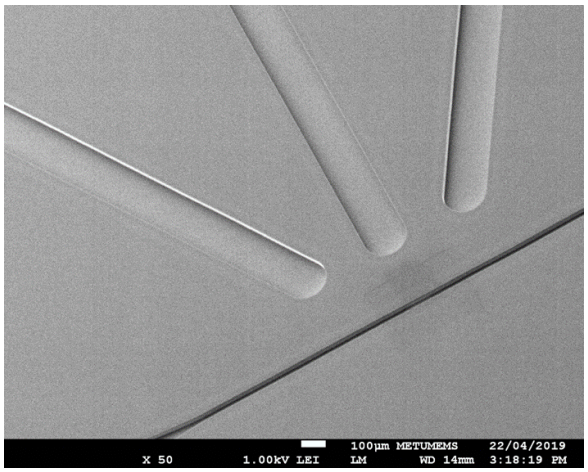

Figure 3.13 SEM image of microchannel and electrode cavities on silicon wafer

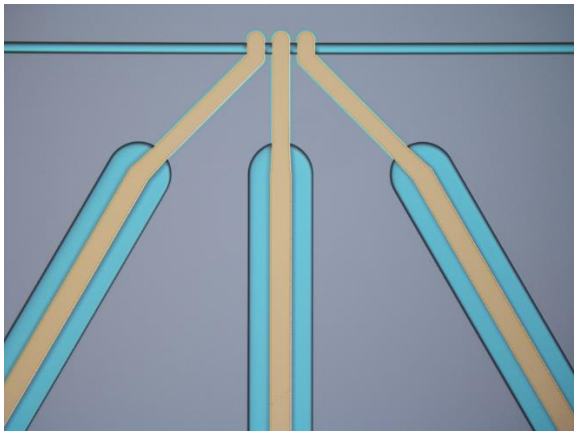

Figure 3.14 Final image of the electrode and channel of the fabricated chip under bright-field microscope

3.3.2 PDMS-Glass Device Fabrication

PDMS Mold Fabrication

In order to fabricate microfluidic channels using PDMS, firstly different fabrication flows were studied. It was decided to use a thick photoresist patterned on a glass or silicon wafer as a mold. For photolithography processes, the DRIE etching mask used in MEMS fabrication was utilized. Thus, there was no need to produce a new mask again. However, when this mask is used with a positive photoresist, the photoresist in the microfluidic channel region dissolves and the photoresist in the

remaining area stays on the wafer surface. It is necessary to obtain the opposite structure in the structures to be used as PDMS molds. Therefore, two different fabrication flows have been developed to obtain this structure.

In the first fabrication flow, the channel pattern was first transferred onto a blank glass wafer using a positive photoresist. Then a 200nm thick Chromium (Cr) film was coated on the wafer and this film was shaped by the lift-off method. Thus, the negative of the channel mask was obtained on the glass wafer. A thick positive photoresist (AZ40XT, thickness 30 µm) was then coated on the Cr film and the wafer was exposed from the reverse side to obtain the mask for the PDMS channel. In the second fabrication flow, the negative of the channel mask was obtained on a glass wafer in the same way. A thick positive photoresist (AZ40XT, thickness 30 µm) was then coated on a silicon wafer and exposed using the glass wafer as a mask. The fabrication steps of both methods are shown in Figure 3.15. The fabricated mold is presented in Figure 3.16.

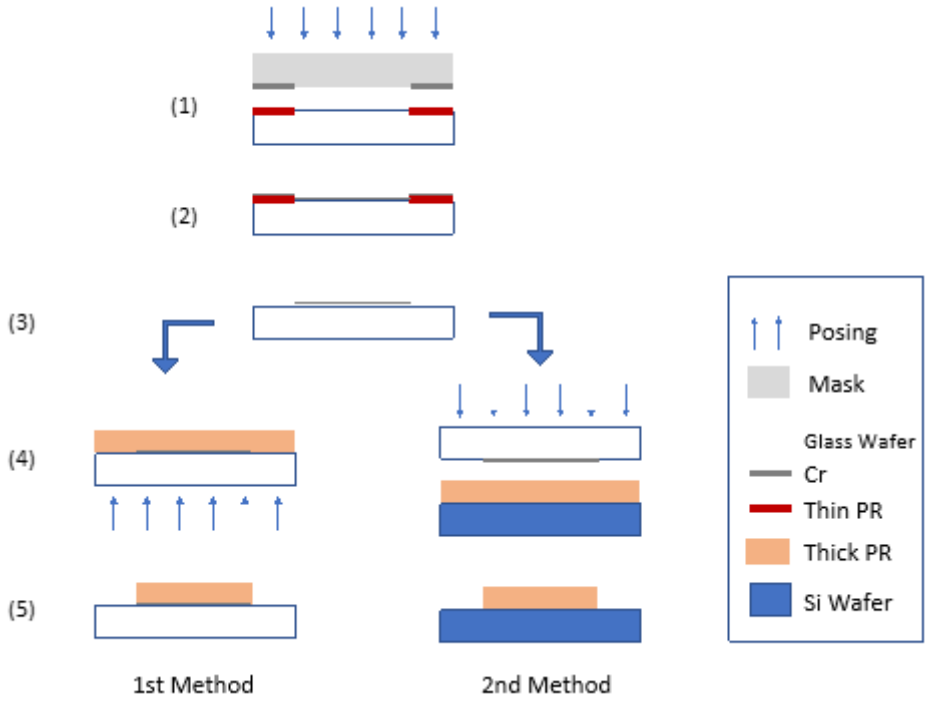

Figure 3.15 Two different fabrication flows used in mold fabrication

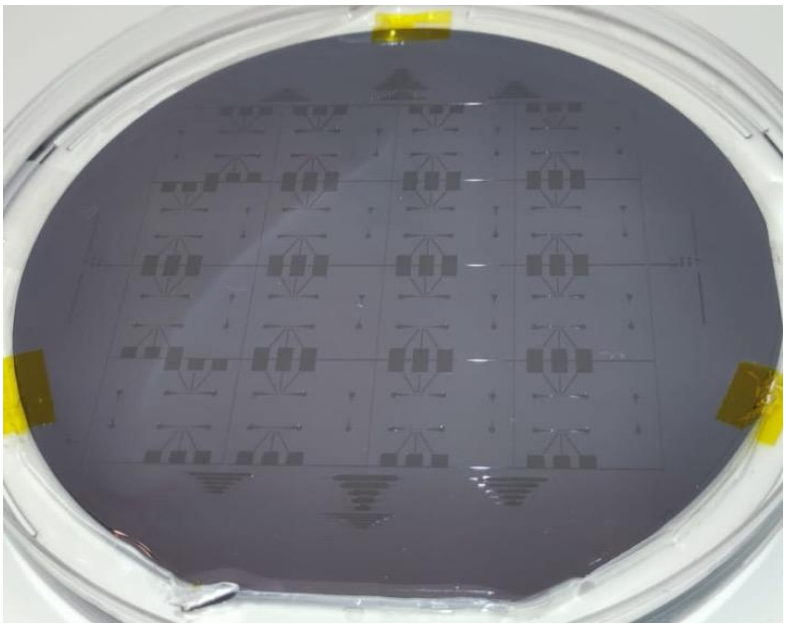

Figure 3.16 Fabricated mold

PDMS preparation and chip fabrication

Polydimethylsiloxane (PDMS) microfluidic chips were produced by a standard molding process (Figure 3.17). First, PDMS and curing agent (Sylgard 184, Dow Corning) are mixed in a 10:1 ratio in a transparent plastic container for 5 minutes. After the solvent is homogeneously dispersed, air bubbles are formed in the mixture. The mixture is then degassed in a vacuum system. This process takes approximately 60 minutes. The degassed PDMS is poured into a mold coated with silane. For the silanization process, the mold and the petri dish containing a few drops of silane are placed in a vacuum chamber and incubated under vacuum for at least 2 hours. After incubation, the mold surface is considered to be coated with silane and ready for the PDMS casting process. The silanization process allows the PDMS to peel off the mold more easily and to avoid damaging the narrow channels. The mold is then placed on a flat surface and the prepared PDMS mixture is carefully poured in. The best way to ensure that the small bubbles in the PDMS do not expand is to cure longer at room temperature. Therefore, the PDMS is cured at room temperature for at least 24 hours. Since the mold has a negative structure, the protrusions on the mold take the shape of the mold as an intrusion on the PDMS and the intrusion on the mold

as protrusions on the PDMS. After curing, the PDMS chips are cut along the edge lines using a sharp blazer and removed from the mold. Pogo pin holes are then punch with a 1.25 mm biopsy punch to contact the electrodes with the inlets and outlets of the microfluidic device to allow fluid entry.

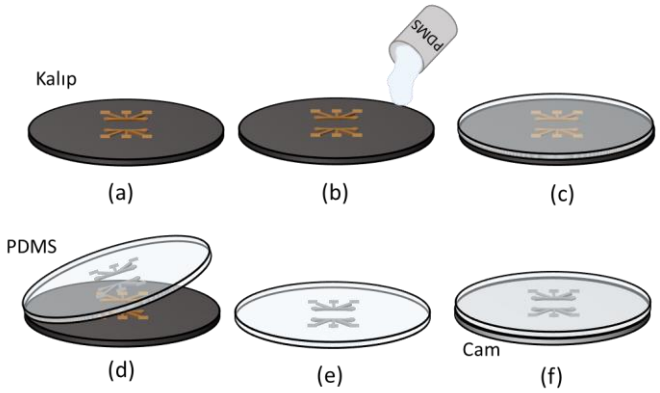

Figure 3.17 Schematic of PDMS chip fabrication a) Fabricated silicon mold b) PDMS casting c) PDMS curing d) PDMS peeling e) Punching of ports f) Bonding of microchannel to glass wafer [43]

The PDMS microchannel is bonded to the glass electrode surface by oxygen plasma treatment. When PDMS comes into contact with the glass surface, a strong covalent bond, Si-O-Si, is formed between the glass and PDMS. This covalent bond between them provides an irreversible seal. Although the plasma treatment only activates the PDMS surface, it can be applied to glass in the same way. In this case, the plasma cleans the glass surface, resulting in better bonding. Before the process, both parts are placed in the plasma device with the surface to be bonded facing upwards. The plasma environment is vacuumed, and oxygen gas is introduced at a flow rate of 26.6 sccm and exposed to oxygen plasma for 20 seconds (Figure 3.18). It is important that the color of the plasma is purple to pink. After the oxygen plasma process was finished, the alignment process during the bonding of the glass wafer with the PDMS containing the microchannel structure was carried out under a microscope. First, the glass wafer was placed on the microscope table and 1 drop of DI water was added on it. The DI water does not disturb the hydrophilic structure of the surface and allows the PDMS chip to be moved on the glass wafer without sticking, thus making

alignment easier. The bonding process is then performed in the position where the microchannel and electrodes meet perpendicular to each other. To increase the bond strength, the chip is placed on a hot plate and kept at 30°C for 30 minutes. Figure 3.19 shows the final fabricated microfluidic device and image under a microscope.

Figure 3.18 Oxygen plasma treatment process

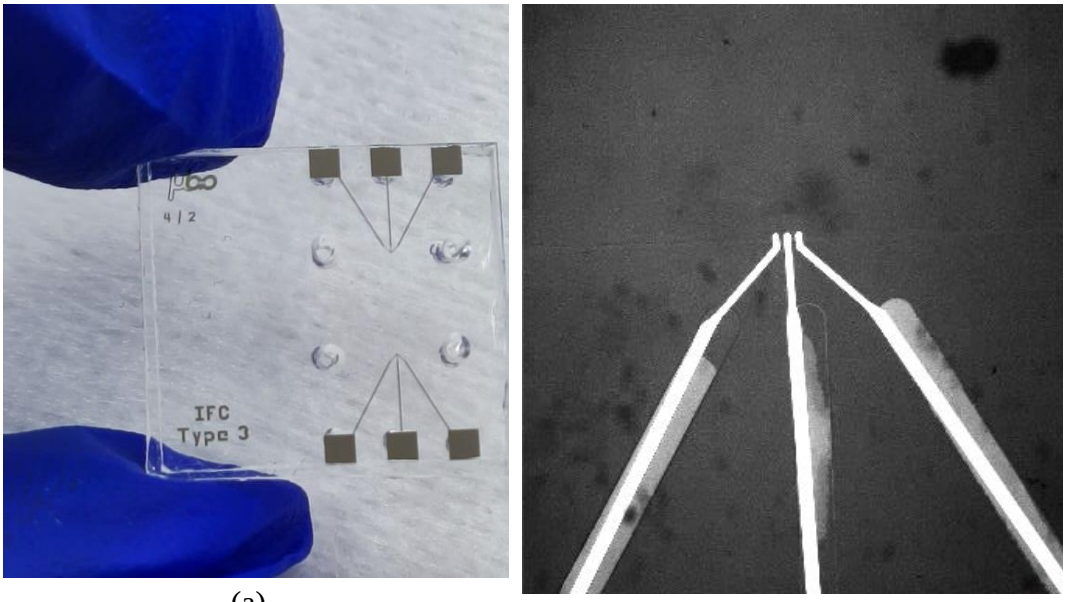

(a) (b)

Figure 3.19 (a)Fabricated PDMS microfluidic device (b) Image of the device under a bright field microscope

3.4 Chip Cartridge

Chip cartridge is aimed to use for ease of operation as it does not need an experienced user and a proper pneumatic setup for operation. It has two main parts, one provides a nest for chip to be placed, other one is the lid that have channels to provide fluid passage through it with two ports that connect to chip. It is manufactured using SLA technique on a 3D printer. Chip nest and lid parts are connected to each other with nuts and bolts. These nuts and bolts also help the sealing of the cartridge.

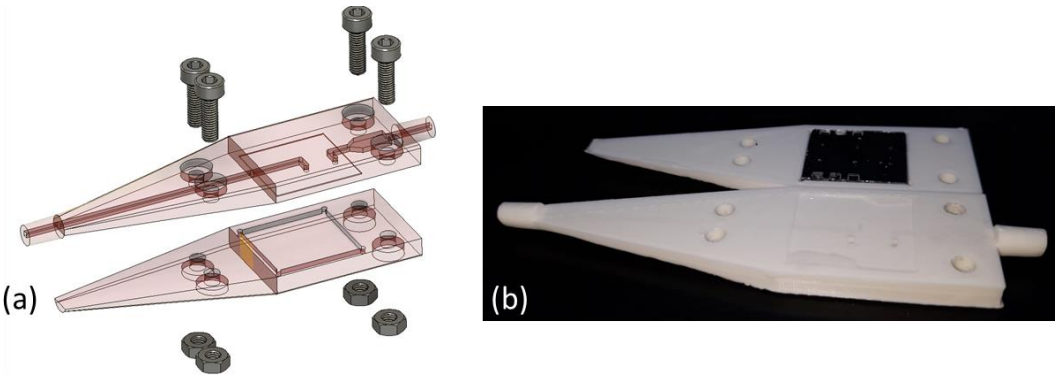

Figure 3.20 Chip Cartridge - Model and Manufacured Cartridge

Cartridge's inlet and outlet ports are standard Luer connections, which allow easy fluidic connection to outer parts. It is planned to be work under vacuum rather than positive pressure.

3.5 Sample Preparation

Two main samples are used for testing of the devices. First one is polystyrene bead solution and second one is cell suspension.

3.5.1 Bead Solution Preparation

Beads that have 6 and 10 µm diameters are used for testing. Polystyrene beads (Polysciences) are used for this purpose. Used beads are fluorescent colored so they

can be seen easily under fluorescence microscope. Solutions are prepared in 1 mL of PBS. Prepared solutions have approximately 500k/mL concentration. Concentration of solutions are adjusted according to cell counter information (BioRAD TC20). To bead solutions, Tween20 (Sigma-Aldrich) is added with %0.5 volume ratio to prevent bead adhesion to microchannel. Three different solutions are prepared for experiments. These are 6 µm, 10 µm and 6 - 10 µm 1:1 mixture bead solution. All solutions are vortexed prior to experiment to provide homogenous distribution within the sample.

3.5.2 Cell Suspension Preparation

As it is explained in section 1.2 white blood cells have two main subtypes: Neutrophils and Lymphocytes. For characterization of the device for these two cell subtypes, they need to be separated from rest of the blood cells and suspension with each of them need to be prepared separately. For separation of lymphocytes and neutrophils from rest of the blood cells a commercial cell separation kit is used. Lymphocytes and neutrophils isolated from whole blood using negative selection principle. Used kits for this purpose are MACSprep HLA B/T Cell Isolation Kit and MACSxpress Whole Blood Neutrophil Isolation Kit. These isolation kits are used according to guidelines provided by manufacturer by trained personnel. At the end of the process, live lymphocytes and neutrophils becomes selected from blood separately. Processed bloods are obtained from volunteers from METU Medical Center. Blood processes are carried out by biologist personnel at Bio-MEMS research group.

In addition to that obtained cells fixed using well-known protocols by trained personnel to be able to store the cells for a longer period time to allow repeated use.

Cell samples are prepared in PBS buffer solution using similar methods as bead samples.

3.6 Experimental Setup and Test Protocol

For Si-Glass and PDMS-Glass devices that are operated under laboratory conditions without use of chip cartridge and PDMS-Glass device that is used with chip cartridge, three different experimental test setups are used. Si-Glass and PDMS-Glass devices' test setups under laboratory conditions without chip cartridge are similar with slight differences. Schematic of basic experimental setup that has been utilized for all devices is given in Figure 3.21.

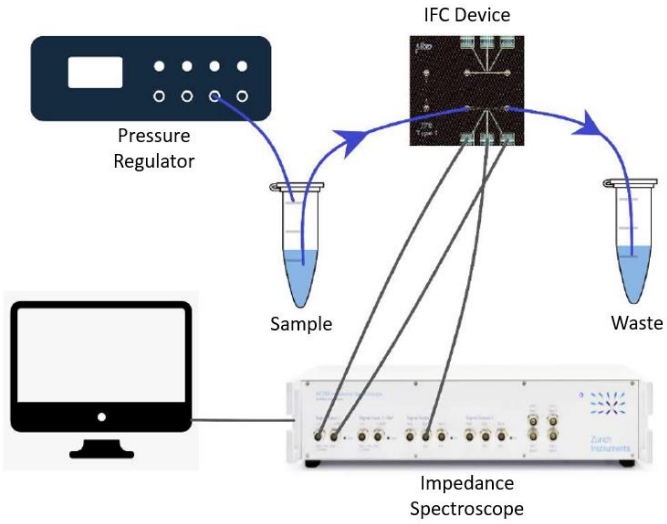

Figure 3.21 Experimental Setup Schematic

3.6.1 Si-Glass Device Experimental Setup and Test Protocol

Photo of experimental setup that is used to test Si-Glass IFC devices are given in Figure 3.22. Experimental setup consists of a microscope, monochromatic high-speed camera, pressure regulator (Fluigent FlowEZ), chip holder that has ports for fluidic and electrical connection, impedance spectroscope (Zurich Instruments HF2IS), current amplifier (Zurich Instruments HF2TA) and a PCB for connecting the Si-Glass device to impedance spectroscope. Fluidic connections of Si-Glass device are made with fused silica tubings and electrical connections are made with BNC cables. Liquids are passed through the device using positive pressure that is

regulated with pressure regulator which is connected to a nitrogen supply. A voltage is created between electrodes and impedance in the microchannel is read with the help of currents that are measured from electrodes in impedance spectroscope.

Prior to sample process, microchannel should be conditioned properly to provide a healthy sample passage through the channel. For this reason, a certain protocol is applied [44]. Initially, ethanol passed through microchannel for degassing purpose. After that, to get rid of the ethanol that is present in the microchannel and tubings deionized water is passed through the channel. After ethanol in the channel replaced with DI water, polymer coating of tubings and microchannel is performed Polymer coating is performed in order to prevent adhesion of cells and microbeads to microchannel and tubings. For polymer coating PEG (PLL (20)-g[3.5]) is used. PEG is applied to the channel as a solution. 0.1 mg PEG is dissolved in 1 ml of DI water to prepare PEG solution. For PEG coating, PEG solution is passed through the system until it fills the microfluidics system completely, then applied pressure from the microchannel is dropped to low levels and left for incubation for 30 minutes. After polymer coating is completed microchannel becomes conditioned and ready for sample passage.

PBS solution is passed from the microchannel firstly after chip conditioning step since sample solution is prepared in PBS. Then, sample is given to system with determined pressure level. As sample passes through the system impedance data is sensed and recorded with impedance spectroscope. When sufficient data is obtained, system is cleaned with detergent solution and DI water.

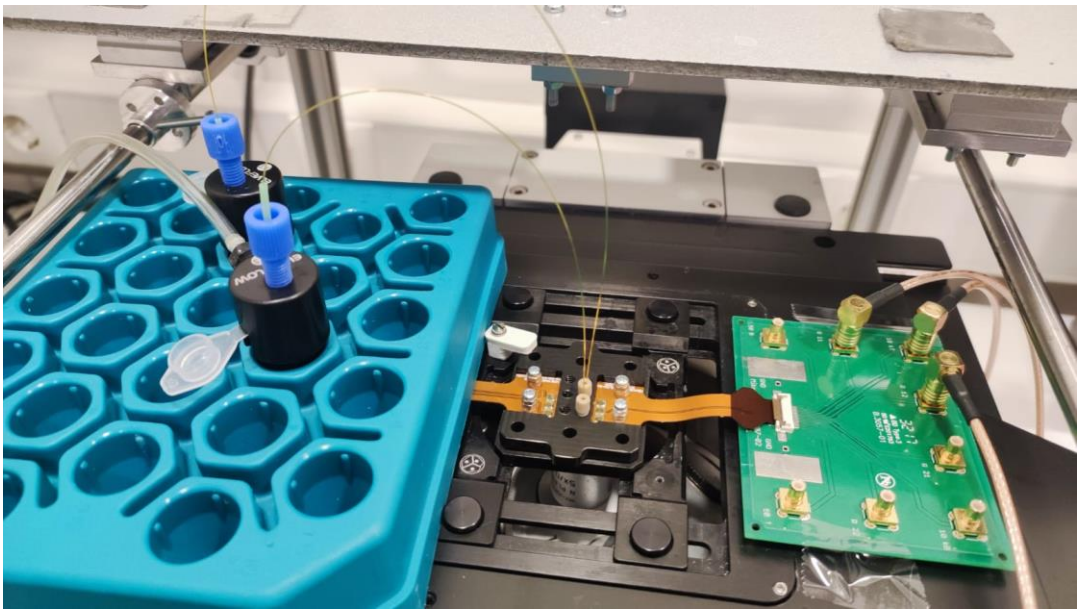

Figure 3.22 Si-Glass Device Experimental Setup

3.6.2 PDMS-Glass Device without Chip Cartridge Experimental Setup and Test Protocol

Photo of experimental setup that is used to test PDMS-Glass devices are given in Figure 3.23. As it can be seen from the figure, PDMS/Glass experimental setup is similar with the Si-Glass experimental setup with some exceptions. First difference between two setups is the lack of chip holder in the PDMS/Glass setup. Since PDMS provides enough resilience to hold tubings in place when used punch diameter to create microfluidic ports on the PDMS channel is smaller than the used tubing at lower pressure levels. Same case holds for pogo-pin connection too. Pogo-pins can tight-fit into the PDMS material and provide stable connection with the device when punch that is used to create electrode ports is smaller than the pogo-pin diameter. Since that is the case in this research, a holder is not manufactured for PDMS-Glass device. However, tubings used for microfluidic connections are changed from fused silica to Teflon tubings for the reasons that are stated above.

Test protocol that is used for PDMS/Glass device is the same with Si/Glass device test protocol.

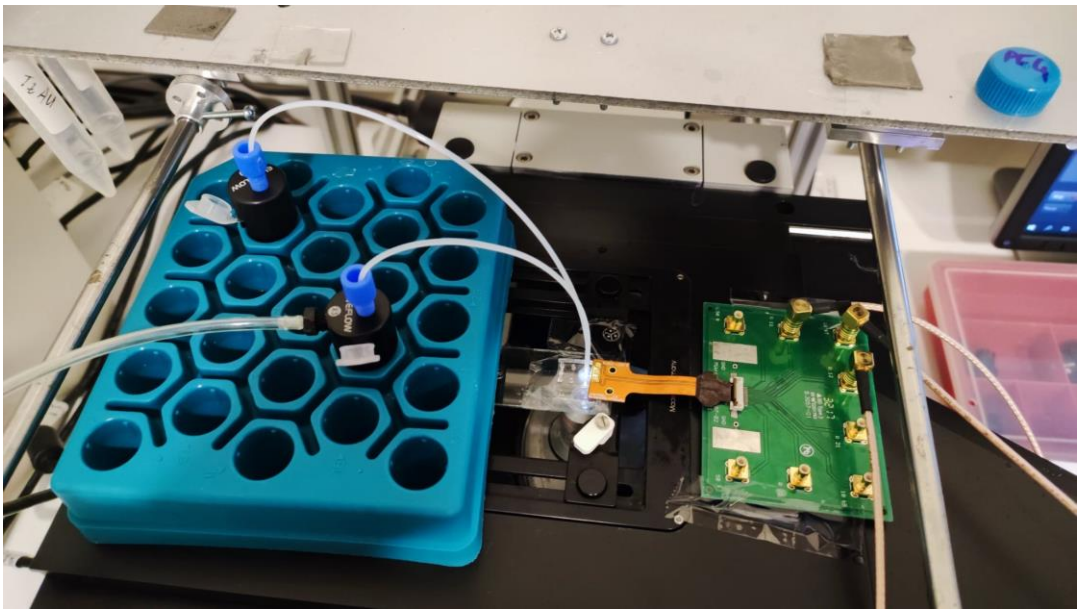

Figure 3.23 PDMS/Glass Device Experimental Setup without Chip Cartridge

3.6.3 PDMS-Glass with Chip Cartridge Experimental Setup and Test Protocol

PDMS-Glass chip cartridge experimental setup consists of chip cartridge and a vacuum source and regulator (Elveflow AF1). Chip is placed and secured to the chip cartridge with help of bolts and nuts. Fluidic connection between sample, device and vacuum source achieved with Luer-Lock connectors and Teflon tubings. Photo of experimental setup with chip cartridge is given in Figure 3.24. Since, no electrical measurement is taken with chip cartridge setup, impedance analyzer and electrical connection units are not utilized.

To test the chip cartridge setup, DI water is passed through the device inside the cartridge with the help of vacuum source and secure flow of the fluid and leakage is checked.

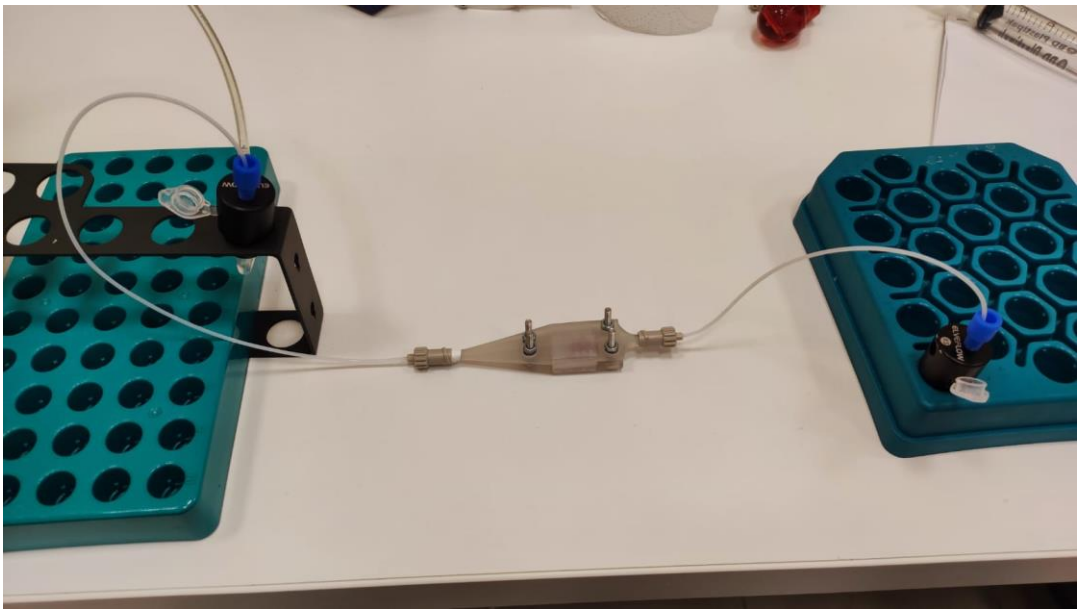

Figure 3.24 PDMS-Glass Device Experimental Setup with Chip Cartridge

3.7 Peak Detection Algorithm

Electrodes of IFC device reads an impedance when microchannel is filled with liquid. Normally, when there is no bead or cell passage above the electrodes, impedance of PBS solution is read through the electrodes with impedance spectroscope. Passage of a bead/cell disrupts this measurement, then measured impedance returns to its base level. This disruption of sensed impedance is characterized by a sharp decrease or increase of the impedance level. This sharp change of the measurement is named as a “Peak”. An example measurement that demonstrates a peak is given in Figure 3.25.

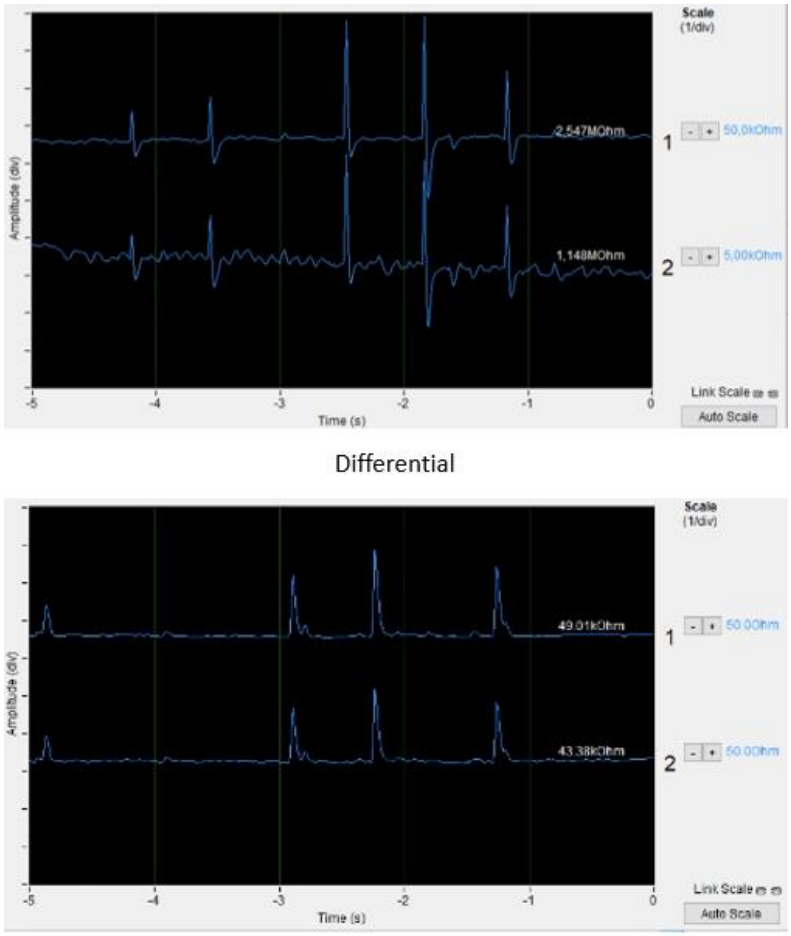

Figure 3.25 Impedance Peaks

Peaks that occur while passage of beads/cells are main characterizing element for detection and discrimination of them. However, a peak's absolute impedance is not utilized for bead/cell characterization, its' deviation from the base impedance is [45]. Information about bead/cell is derived from amplitude of the peak that is generated while that bead/cell passes.

Impedance spectroscope records time and current data during the experiment for each used measurement frequency. To analyze these data a peak detection algorithm is developed in MATLAB. Algorithm that is developed requires user input to function properly. Main two inputs are voltage and peak detection amplitude threshold. Algorithm uses voltage input and current data to get measured impedance

vs. time. As it is mentioned, peaks appear above a base impedance so, directly using peak's maximum amplitude is not applicable. Before that a signal processing algorithm should be run in the peak detection algorithm to determine peaks' deviation from the base impedance that is measured in the channel. Aforementioned signal processing algorithm pull the base impedance to zero level, after this process peaks' maximum amplitudes become the desired peak amplitude to be utilized in experiment analysis. This process called baseline removal.

After baseline removal process remaining peaks are compared with user-input peak detection amplitude threshold. This threshold is determined by the user. Users try to detect the minimum peak amplitude that occurs at the instant that a bead/cell passes above the electrodes in the channel. Peak detection algorithm then detects peaks that have larger amplitude than the threshold input. Users can observe the channel during an experiment with the help microscope camera so, they can match peaks with bead /cell passage. This process is necessary because some ghost peaks can occur during an experiment. A ghost peak is called a peak that occurs without the effect of a bead/cell. Other than ghost peaks, also sometimes measurement obtained from the impedance spectroscope can be noisy to some level that an instant of baseline impedance can appear as a peak. These noises also need to be removed since they are not real peaks. Because of these reasons, users try to detect a minimum peak amplitude that bead/cell passage causes. Detected peaks after a run is given in Figure 3.26.

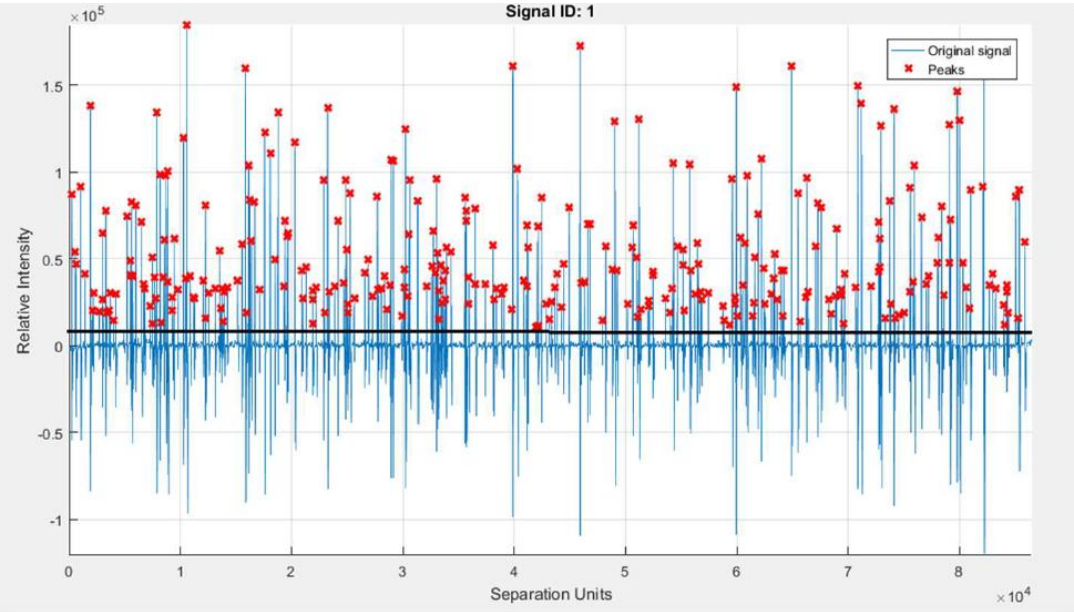

Figure 3.26 Detected Peaks at Peak Detection Algorithm

Another safety mechanism that is used to ensure a peak really caused by a bead/cell, but it is not just a spike that occurs randomly is comparing the instants that peaks are detected between two frequency levels. It is assumed that if a peak is created by a bead/cell it should create a peak for each frequency. Peak detection algorithm runs for measured two frequencies and detect peaks for each of them. After that, algorithm tries to find a match for each peak at a frequency with a peak that occurs at that time at the other frequency. If a peak pair is found for each frequency, then those two peaks are considered real, created by a bead/cell, and they are saved. But if, for a peak at one frequency, no match is found at the other frequency; then that peak is considered as noise/ghost peak and discarded. This algorithm runs for each frequency for all of the peaks and at the end low and high frequency peak amplitudes for each detected bead/cell that passes through the channel are obtained.

These obtained peak data needs to be converted into data of interest for analysis. These data of interest are opacity and bead/cell radius. Opacity is a parameter that is used to normalize the vertical position of beads/cells in the channel [46]. Opacity of a bead/cell is calculated with following formula:

$$Opacity = |Z_{HF}|/|Z_{LF}| \text{ [28]} \quad (3.4)$$

Size information of a bead/cell is derived from its low frequency impedance amplitude [47]. At low frequency cell membrane acts as a barrier, so impedance of a bead/cell is directly proportional with bead/cell size. Bead/cell can be considered as a sphere. So, its size is proportional to cube of its radius. In order to make a relation between low frequency impedance data and bead/cell radius, cube root of average of all low frequency impedance data is calculated. Then, this value is divided into known average radius of bead/cell that is used, and a constant "K" is obtained. This K value relates cube root of low frequency impedance data with bead/cell radius. Another K constant is also calculated for other bead/cell type and average of these two constants is calculated. Average K constant is the common constant to be applied all two different bead/cell type. Common K is applied two both datasets and radius for all detected bead/cell is calculated with that. Relationship between low frequency impedance and bead/cell radius can be summarized as follows:

$$K_{6\mu} = [(\sqrt[3]{Z_{6\mu LF}})_{avg.}]/\, r_{6\mu} \quad (3.5)$$

$$K_{10\mu} = [(\sqrt[3]{Z_{10\mu LF}})_{avg.}]/\, r_{10\mu} \quad (3.6)$$

$$K_{avg.} = (K_{6\mu} + K_{10\mu})/2 \quad (3.7)$$

Then, derived opacity and radius data are plotted to a scatter plot. Also, bead/cell radius histogram is plotted. MATLAB code for histogram and scatter plot generation is provided in Appendix B.

CHAPTER 4

RESULTS AND DISCUSSION

Test results are given in following sections.

4.1 Flow Rate Determination

There is no sensor to measure the flow rate in the test setup used in the experiments, so the flow rate of the sample passing through the microfluidic channel is not known. The reason why there is no sensor to measure the flow rate in the test setup is that the operation flow rates are very close to the lower limits of the flow sensor and the sensor cannot take an accurate reading at these flow rates. Therefore, the flow rate at which the test setup should be run is determined by the positive pressure given to the system from the pressure regulator. This pressure value is visually adjusted according to the rate of passage of microbeads through the channel. However, it has been observed in the experiments carried out in different test setups that different pressure values should be used to obtain same flow rate. Since characterization was not possible before each experiment, a pressure-flow rate curve was drawn for the test setup used and the flow rate was calculated by linear fit method.

The test setups used to characterize the flow and pressure are given in Figure 4.1. Tests were performed in two different setups. As can be seen in Figure 4.1.a in the first installation, the liquid is supplied to the chip with the pressure regulator and a high precision flow meter (Bronkhorst mini CORI-FLOW™ ML120V00) is connected to the output of the chip. The sensor used can measure from 1.6 µL/min to 3.3 mL/min in the range of 0.2%-2% margin of error.

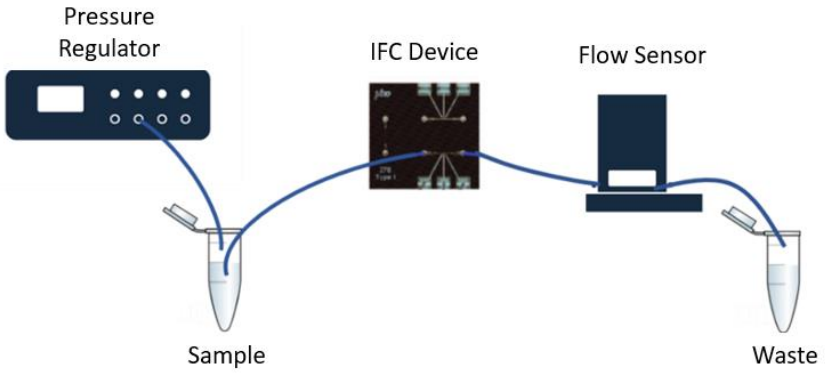

(a)

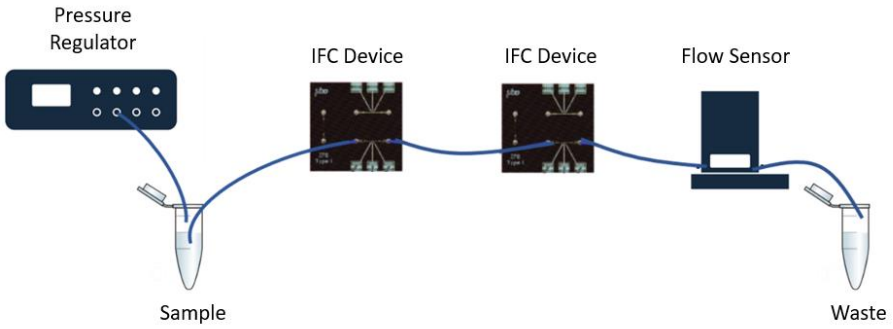

(b)

Figure 4.1 Test Setups Used to Create Flow Rate-Pressure Curve (a) First Setup (b) Second Setup

In the second setup, the total resistance in the system is increased by adding another chip with the same channel size to the output of the chip. At certain pressure values from 0 mbar to 2000 mbar, measurements were taken for about 10 seconds after the flow rate was fixed. Thus, the flow rate values obtained against the applied pressure were recorded. While constructing the P-Q curve, the sensor data recorded for 10 seconds was averaged and a linear trend line was applied to the obtained data set. The measurement curve in the range of 20-200 mbar for the first experimental setup is presented in Figure 4.2.

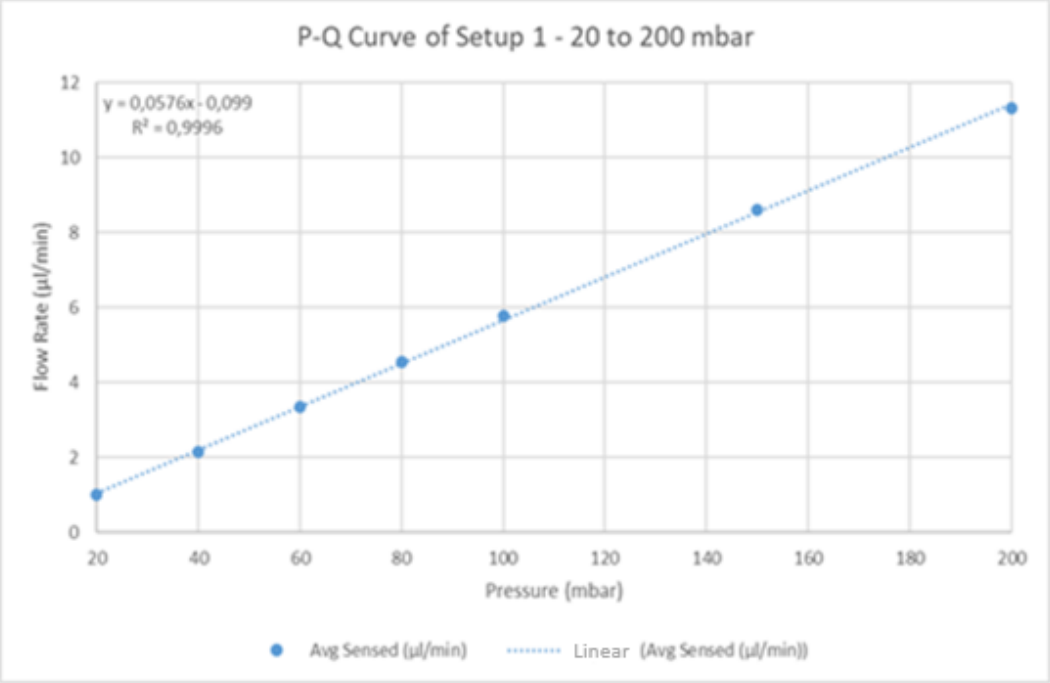

Figure 4.2 Flow Rate-Pressure Graph Obtained Using the First Test Setup

The graphic presented in Figure 4.2. is also compared with the video analysis method. By analyzing the video images of the particles passing through the channel, the flow rate in the channel was calculated as 0.3 µl/min when 8 mbar pressure was applied. With the linear fit method applied in the selected range, 8 mbar pressure and 0.36 µl/min flow rate should be obtained. It is thought that the difference of 0.06 µl/min is due to the error margin read by the flow sensor and the trend line applied to the recorded data set.

The graph and linear regression equation obtained in the second test setup are given in Figure 4.3. In this setup, another chip in series with the same channel size is added to the output of the used chip in order to increase the total resistance in the system. When the graph in Figure 4.3 is examined, it is seen that the pressure required to obtain the same flow rate is approximately 2 times compared to the test using a single channel. When deemed necessary, by increasing the total resistance of the system, the pressure regulator and -if used- flow sensors can be operated at a safer and farther point from the lower limits of their operating values.

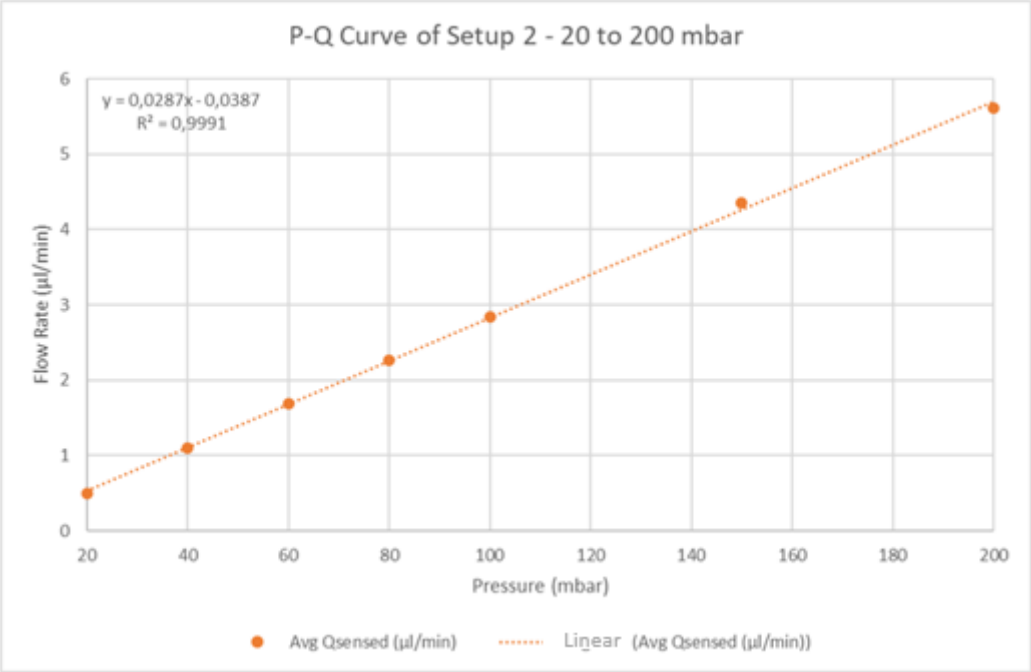

Figure 4.3 Flow Rate-Pressure Graph Obtained Using the Second Test Setup

4.2 Frequency Sweep Results

For device characterization and to determine the signal frequency that is to be used in cell and bead flow experiments, Absolute Impedance vs. Frequency and Phase vs. Frequency response curves are obtained between 10 kHz and 10 MHz frequencies. As it is mentioned, two frequency measurement needs to be taken to gather two types of information about the cell. Low frequency measurement should provide information about cell size, since at low frequencies cell membrane act as a barrier, thus measured impedance provides information about cell size. On the other hand, high frequency measurement should give information about cell interior, cytoplasmic content. The reason for that is high frequency signals can perturbate cell membrane and creates a response that depends on cytoplasmic contents of the cell [26].

However, in microchannel impedance measurement, cell is not the only factor that determines the measured impedance. At low frequency levels double layer

capacitance is the main factor that determines the impedance response of the IFC device [27]. So, as it is stated in the literature, at lower frequencies double layer capacitance dominates the impedance measured in IFC system.

As double layer capacitance dominates the impedance at lower frequencies, at higher frequencies another factor that comes into play. Parasitic capacitances arise from the direct coupling between the two electrodes. At high frequencies they are the main factor that is responsible for impedance that is sensed. Other factors are negligible [48].

Between the frequency levels where double layer and parasitic capacitances are the main determining factor of measured impedance, there is a resistive frequency spectrum where impedance measured in the channel is not affected by double layer and parasitic capacitances significantly [49]. This region is called plateau and it is characterized by a section where impedance stays constant or does not change significantly among certain frequencies. For a utilizable impedance measurement to be taken, used frequencies at IFC system should be between these frequencies. Otherwise, as it is mentioned, effect of cell on the impedance would not be observable.

To be able to detect available working frequency range, impedance of the IFC device should be measured between a frequency interval. For this reason, frequency of the system swept from 10 kHz to 10 MHz and absolute impedance between these frequencies recorded. To be able to check the available designs, same test repeated for Type 1, Type 2 and Type 3 designs. Prior to measurement microchannel is conditioned according to protocol given in chapter 3.6. Measurement taken while channel is filled with PBS solution. Both PDMS and Si-Glass devices are tested.

Obtained measurements for different designs are given in Figure 4.4.

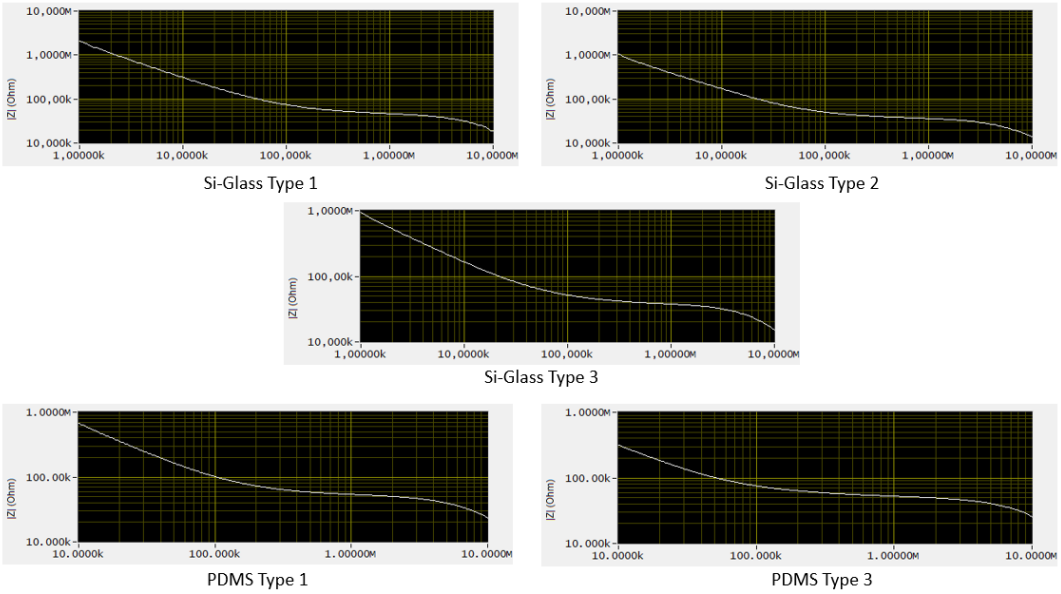

Figure 4.4 |Z| vs. Frequency Results of Different IFC Devices

If Figure 4.4 is examined, it can be seen that at all devices resistive plateau region lies between similar frequency intervals. Around 400 kHz – 3 MHz all devices have a plateau region. In addition to that data, literature is also checked to determine the working frequencies of the IFC device [26], [27].

As a result, 470 kHz and 2 MHz frequencies are selected as low and high frequency levels respectively to utilize in the bead/cell experiments.

4.3 Leakage Experiments

During experiments, while liquid flow is in place, air-liquid interfaces are observed at electrode cavities in Si-Glass devices. An example image obtained under microscope of these air-liquid interfaces are given in Figure 4.5. Reason of this leakage could not be identified clearly. Apart from that, whether this leakage causes a problem during experiments or not, could not be detected while performing measurements.

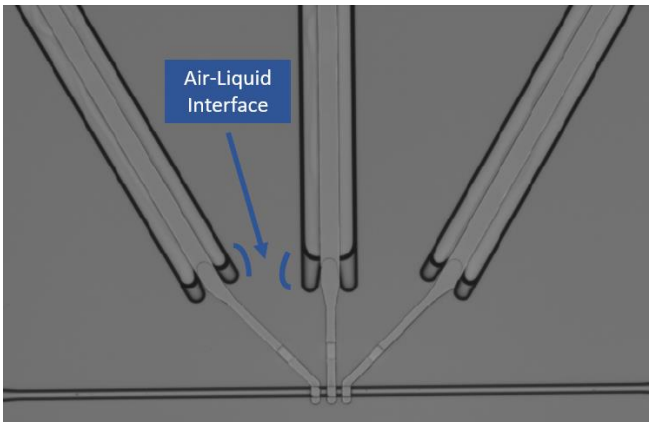

Figure 4.5 Air-Liquid Interface

Firstly, if leakage can be avoided with using operating pressures below a certain threshold is decided to be tested. In order to observe that, an experiment is planned with fluorescently stained DI water and ethanol. At this experiment, applied pressure while passage of DI water and ethanol is increased gradually to detect a point where leakage to electrode cavities begin to occur. Also, even while using lower pressure values, if application of pressure at extended times still causes leakage to occur is decided to be tested.

Images obtained are experiment is given in Figure 4.6. As it can be seen from the images gradual increase of applied pressure for ethanol and DI water causes leakage of passing liquid from the microchannel to electrode cavities. Leakage observed for both liquids at similar pressure values, around 300 mbar. However, performing an experiment below these pressures, especially during conditioning phase, is not ideal.

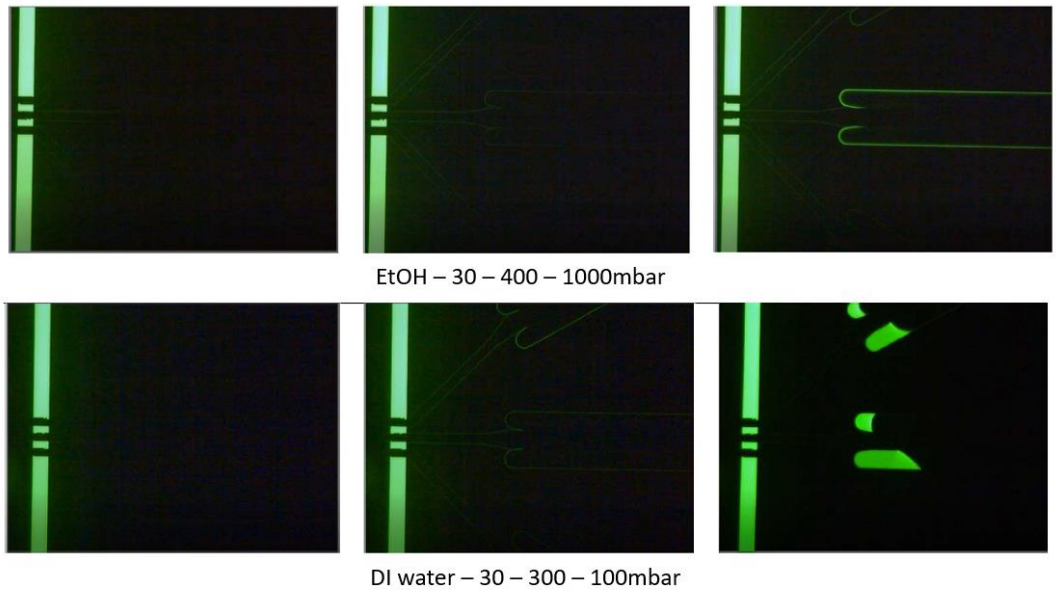

Figure 4.6 Si-Glass Device Leakage Test

Cross section of the Si-Glass device is examined under SEM. SEM image is given in Figure 4.7. Unfortunately, no possible leakage reason could not be identified with these inspections. Intuitively, reason of the leakage is thought as bonding of two hard materials could not provide a satisfactory sealing to prevent liquid passage. Due to this reasoning, it is thought that a better sealing may be achieved at PDMS-Glass devices.

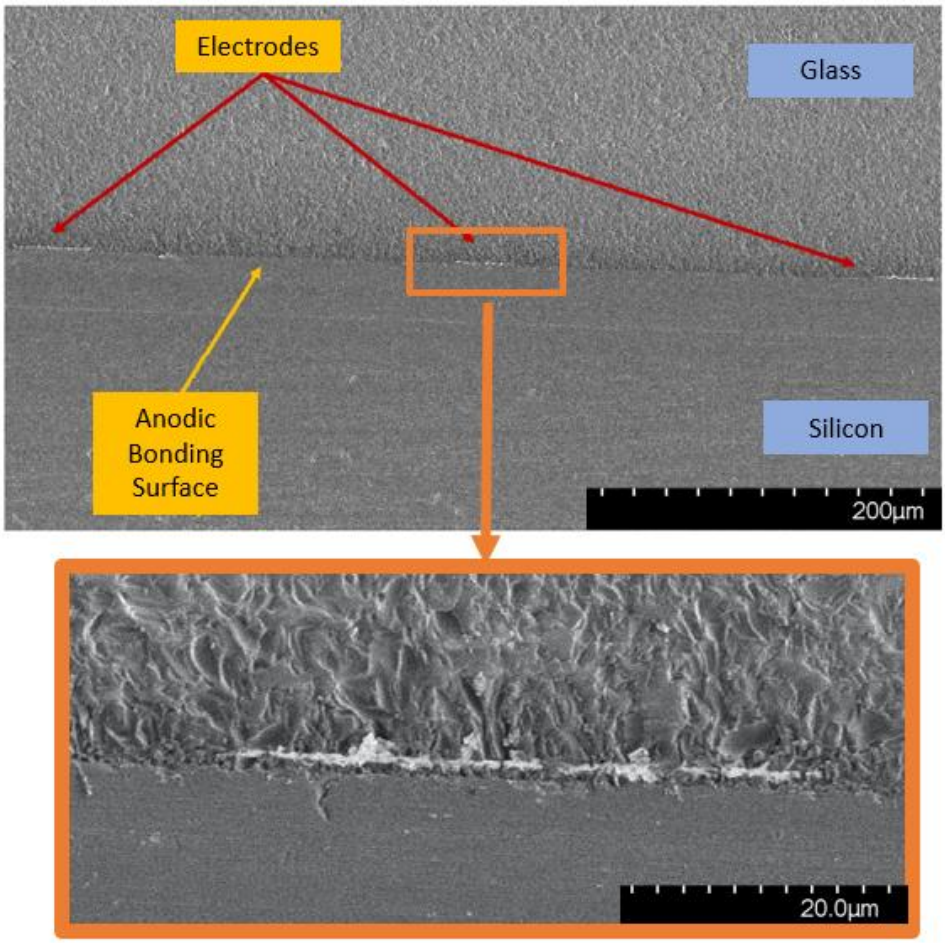

Figure 4.7 SEM Inspection of Si-Glass Device Bonding

Same leakage test performed for PDMS-Glass devices. An image captured during this test is given in Figure 4.8. No leakage outside to microchannel is observed during this test. Test lasted 5 minutes. Maximum 3000mbar of pressure is reached during this test which is way higher than the pressure required for IFC operation.

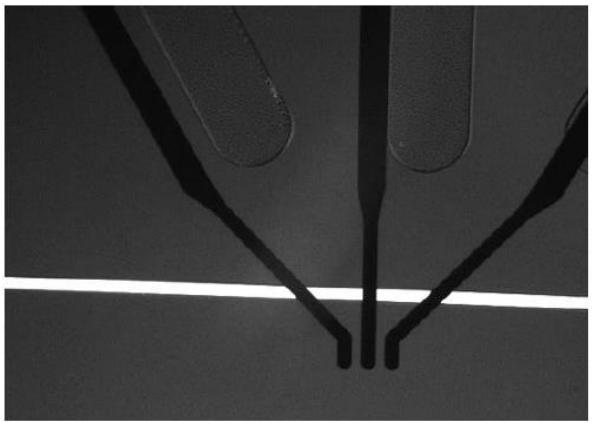

Figure 4.8 PDMS-Glass Device Leakage Test

As a result, since leakage issue at Si-Glass devices could not be avoided, it is decided to carry on the experiments as it is.

4.4 Bead and Cell Flow Impedance Analysis Results

As it is mentioned in section 3.5. two main samples are tested using the device fabricated. Impedance data is saved while they are passing through the micro channel and peaks are obtained from this data with the help of peak detection algorithm as it is described in chapter 3.7. Their detailed analysis is given in following sections.

4.4.1 Bead Sample Impedance Analysis

Beads that have 6 and 10um diameters are passed separately and together through the channel. All experiments are conducted according to protocols given chapter 3.5 and 3.6. All analysis are performed with the help of peak detection algorithm that is described in chapter 3.7.

4.4.1.1 Si-Glass Chip Bead Sample Results

Experiments with Si-Glass devices are decided to be carried out in two major sets. First set is aimed to determine the optimum design that is available among the

designs that are fabricated. Second set is aimed to check repeatability of the results with increasing number of experiments among with testing possible improvements, changes related to test protocol to improve the performance of the device.

For the first set, Type 1 – 2 and 3 devices are used. 8 mbar pressure is used as operating pressure. This pressure is chosen because initial trials showed that increasing pressure above this point may cause IFC device to miss some of the beads, especially at differential measurement. 2 experiments are conducted for each device type.

Criteria to select better design are determined as follows: First one is true detection percent. Used beads for tests have 3 and 5 µm radiuses respectively. At this stage only size-based separation is decided to be implemented. Since opacity is a normalizing factor and also theoretically high frequency impedance data should not provide additional information about beads since they are polystyrene solid particles [50]. For size-based differentiation correctness criteria a threshold radius is determined. This threshold radius is determined as 4 µm since it is middle point of two used bead radius. Calculated radiuses of beads are checked if they are below or over the threshold radius. That is to say if a 6 µm bead's electrical radius is below the threshold 4 µm radius it is considered as true detected, but if it's electrical radius is above the threshold it is considered as false detected. Similar case is valid for 10 µm beads. As it is mentioned in the beginning, in one case different size beads passed through separately. So, distinguishing different bead data exactly from each other is possible.

There are two main types of measurements that can be taken with this IFC device. First one is single ended, second one is differential measurement. A simple diagram showing the measurement method is given in Figure 4.9.

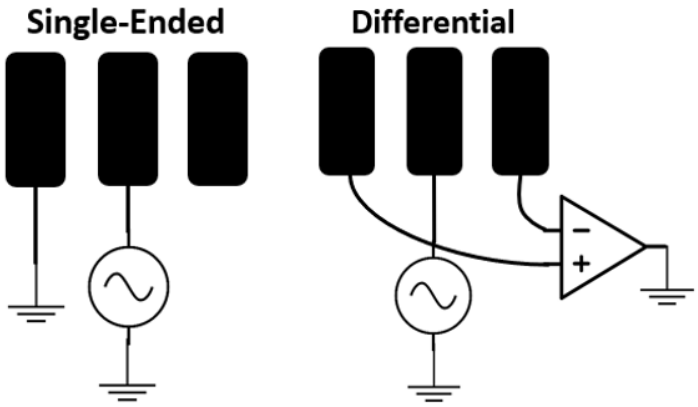

Figure 4.9 Differential - Single Ended Measurement Diagram

As it can be seen in the diagram, differential measurement takes current measurement from two laterally positioned simultaneously, takes difference of them, and measures the impedance from this data.

Middle electrode is excitation, and two side electrodes are measurement electrodes on this system. Beads enter one side of the channel and pass above the electrodes in order. At the instant bead passes through the first measurement electrode, first electrodes read data of bead suspended in the channel solution and second measurement electrodes reads data of the solution filling the channel only. By subtracting these two data from each other, we can get rid of the effect of PBS solution in the channel. So, resulting impedance becomes solely created by bead that passes. A figure that illustrates is provided in Figure 4.10.

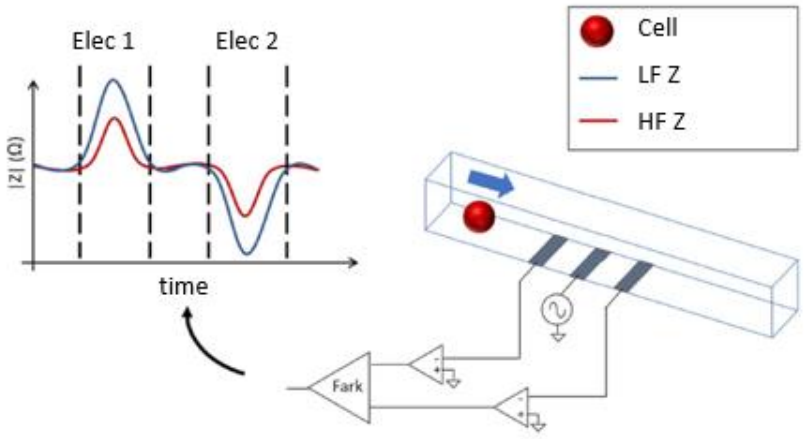

Figure 4.10 Differential Measurement Principle

Other measurement method is single-ended measurement. In this measurement type, only two electrodes are used. Similar two differential measurement, one electrode is excitation, and one electrode is the measurement electrode. Impedance created is related with channels whole content all the time, there is no current differentiation is made. Since only two electrodes are used in single-ended measurement and there are three electrodes available in the design an extra geometry can be tested with single ended measurement. First one is the original design where middle electrode is the excitation electrode and one of side electrodes is the measurement electrode. Second configuration that can be used is using one side electrode as excitation and other side electrode as measurement electrode. By utilizing this a new electrode geometry emerges automatically with same electrode widths and larger electrode spacing. This new electrode spacing is equal to two times the original spacing added to one electrode width.

Screenshots from HF2IS user interface from different measurement types are given in Figure 4.11. Thresholds for peak detection are determined by the user according to these information. 470 kHz used as low frequency; 2 MHz used as high frequency value. 1 Vpp is applied as excitation voltage. 14400 sa/s used as sample acquisition rate.

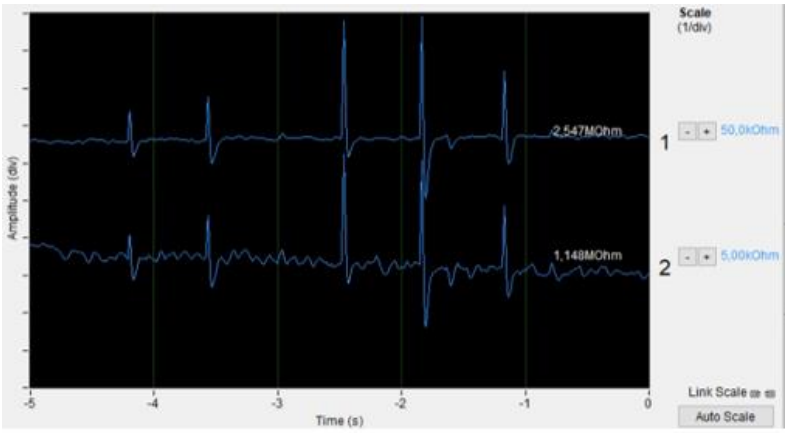

Differential

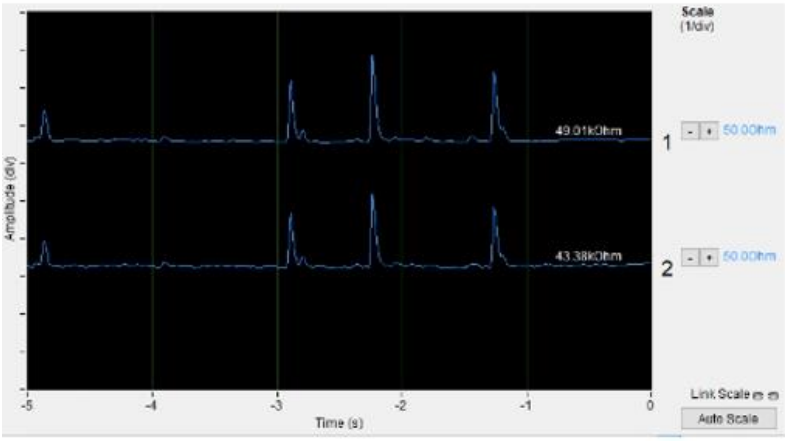

Single - Ended

Figure 4.11 Differential - Single Ended Measurement HF2IS UI

At differential measurement two peaks (one positive, one negative) appear for one bead. Both of positive and negative peaks analyzed separately to compare their correctitude in terms of results to select the better option in further experiments. Differential measurement also taken in both ways that is to say both electrode 1 – electrode 2 and electrode 2 – electrode 1 configurations are tested to select better option in further experiments. Single ended measurements also taken in short (side electrode: measurement, middle electrode: excitation) and long (one side electrode: measurement, one side electrode: excitation) configurations.

6 and 10µm beads data is collected separately. At post processing, peak detection algorithm stage for each bead group a constant to relate low frequency impedance

cube root with cell size is obtained. Ideally this constant should be equal for 6 and 10µm beads since the relationship between cube root of impedance data and bead radius is linear [51]. However, experimentally derived constants for 6 and 10µm can be different from each other. So, average of those two derived constants are calculated and this average constant is applied to both 6 and 10µm beads' data. By this way, even those two beads data is taken separately, they can be analyzed as if they are given to the device as a mixture.

Obtained average results for two experiments of this set is given in Table 4.1. Values in table are color coded to simplify analyzing the results. Color codes and their meanings are also provided in the same table.

Table 4.1 Si-Glass Set 1 Bead Type Comparison Experiments Results

		# True Detected 6u	# True Detected 10u	% True Detected 6u	% True Detected 10u	% Std.Dev/Mean
Type 1	1-2 Pos.	89	68	79,5	65,4	24,528
	1-2 Neg.	32	99	91,4	64,7	30,677
	2-1 Pos.	13	26	100,0	83,9	9,340
	2-1 Neg.	42	104	79,2	49,1	38,697
	1 short	91	200	75,8	46,1	33,145
	1 long	167	363	91,8	76,9	19,410
	2 short	60	51	62,5	26,0	38,484
	2 long	170	140	89,0	76,5	17,814
		# True Detected 6u	# True Detected 10u	% True Detected 6u	% True Detected 10u	% Std.Dev/Mean
Type 2	1-2 Pos.	39	38	79,6	38,4	40,046
	1-2 Neg.	30	43	81,1	26,9	48,686
	2-1 Pos.	53	25	70,7	43,1	23,760
	2-1 Neg.	95	47	78,5	61,0	23,620
	1 short	81	80	75,7	63,5	25,913
	1 long	NA	NA	NA	NA	NA
	2 short	79	93	88,8	100,0	22,498
	2 long	NA	NA	NA	NA	NA
		# True Detected 6u	# True Detected 10u	% True Detected 6u	% True Detected 10u	% Std.Dev/Mean
Type 3	1-2 Pos.	21	15	72,4	83,3	27,781
	1-2 Neg.	85	67	81,0	71,3	25,074
	2-1 Pos.	98	105	83,1	56,8	28,373
	2-1 Neg.	118	121	80,8	57,1	25,288
	1 short	112	59	75,2	47,6	28,283
	1 long	44	86	83,0	68,3	17,283
	2 short	130	112	78,3	51,9	26,055
	2 long	57	101	86,4	63,5	16,043

Color Codes		
Detection <%60	%60 < Detection <%80	%80 < Detection
# < 60	60 < # < 100	100 < #
% Std.Dev/Mean > %25	%25 > % Std.Dev/Mean > %10	%10 > % Std.Dev/Mean

All measurements are taken at durations which allow at least around 90-100 beads passage to be completed to make it possible to check designs not only differentiation but also detection capabilities. Standard deviation/mean values are given also to check dispersion of calculated radiuses of detected beads.

If we should analyze set 1 results, at first glance it can be said that Type 1 and 3 showed better results than Type 2 device. In almost all measurements Type 2's success rate fall behind other two types. If we go further and compare Type 1 and 3 together, either of the designs' performances do not exceed the other by a significant amount. But taking into account true detection percentages, it can be said that Type 3 stands out a little more especially taking into account single-ended measurement results, so further tests are decided to be carried out using Type 3 devices, which is also concordant with the simulation results obtained at the design stage. An example opacity vs radius scatter plot of Type 3 is given in Figure 4.12. As it can be interfered from the graph, differentiation between two bead groups is possible to a certain degree.

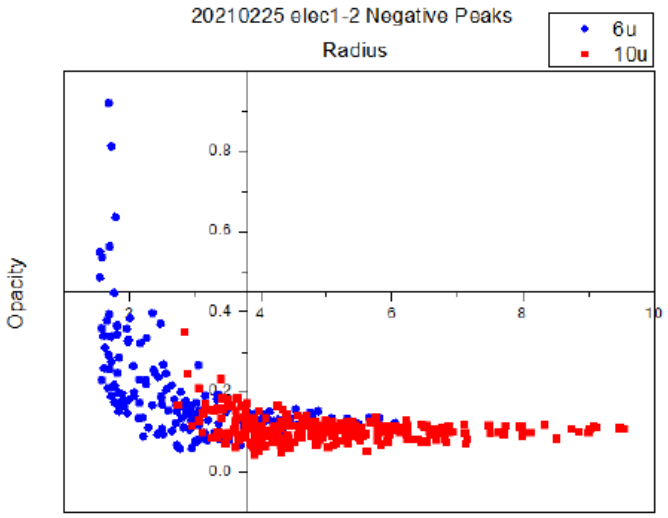

Figure 4.12 Example Opacity vs Radius Scatter Plot - Si-Glass - Type 3

For possible reasons of the inconsistency of the measurements a few ideas come to mind. First and most probable reason is flowing of beads at different z heights. Currently used IFC design does not have any focusing mechanism to keep beads

flow at a certain height. There is a strong possibility that beads flow at random heights along the channel z plane. This can cause a considerable amount of deviation in measured impedance that occurs due to beads. There are literature findings that supports this claim [39]. This randomness of bead z position may change from experiment to experiment due to unidentifiable changes may occur between experiments since used setup is not a fully robust experiment setup.

Second possible reason is the leakage of liquids to electrode cavity. Leakage problem that is observed is addressed in prior sections. Results of that leakage tests show that, even a air-liquid interface is not observed by the user under bright field imaging, leakage can still occur to the electrode cavities. No correlation observed between the amount of liquid that leaked and measurement health, but it is safe to say that leakage inserts a uncontrollable and unidentifiable concern regarding the measurements.

Third possible reason is due to Si-Glass fabrication method. Electrodes lies in a cavity on the glass wafer and oxide layer is deposited on top of the regions where electrodes may touch the silicon wafer, however still possibility of electrode to get contact with silicon substrate arises questions. Isolation of electrode and silicon wafer may change from die to die due to possible fabrication inconsistencies.

Fourth possible reason is the noise that is coming from measurement method. Especially in differential measurement this noise or inconsistency in the measurement may alter the impedance measured gravely. In ideal conditions, if there is no mismatch is present in the system, impedance that is measured when there is no bead passage in the device should converge to infinity since current both side sensory electrodes are reading should be the same. In the real system, base impedance is very high, but it can change from experiment to experiment, sometimes even during the same experiment due to unknown factors. This discrepancies or noise in the measurement can influence the measurement negatively.

4.4.1.2 PDMS-Glass Chip Bead Sample Results

Experiments made on PDMS-Glass chip using bead samples. Sample analysis and experiment process is same with Si-Glass devices. Only Type 3 design is tested with PDMS-Glass devices since it is selected as the best working design in Si-Glass tests. Obtained results for a number of experiments is given in Table 4.2. Working pressure of these experiments is determined as 6mbar because by inspection, flow velocity obtained for beads at 6mbar is determined to be equal to flow rate obtained with 8mbar during Si-Glass experiments. Reason of this pressure change is due to tubing change in PDMS-Glass devices. Used tubings inner diameter is larger than the tubings used with Si-Glass devices. Differential measurement only taken in elec1-elec2 configuration and only positive peaks are inspected since no significant difference between using different configurations and peaks is observed in Si-Glass devices. For single ended measurement only original (short) configuration is applied. Example scatter and histogram plots are given in Figure 4.13 and 4.14.

Table 4.2 PDMS-Glass Device - Type 3 - Bead Experiment Results

		# True Detected 6u	% True Detected 6u	# True Detected 10u	% True Detected 10u	% Std.Dev/Mean	Kavg
Exp 1	Diff 6mbar	11	41	0	0	15,7	19,39
	Sing 6mbar	139	97	103	99	11,4	1,09
	Mixture Diff 6mbar	16	107	14	93	12,3	11,92
	Mixture Sing 6mbar	94	107	81	93	12,3	1,12
Exp 2	Diff 6mbar	89	77	44	28	25,8	16,15
	Sing 6mbar	97	84	105	68	18,9	1,02
	Mixture Diff 6mbar	91	132	47	68	22,6	15,86
	Mixture Sing 6mbar	110	118	76	82	14,3	1,10
Exp 3	Diff 6mbar	202	90	156	64	16,6	1,09
	Sing 6mbar	NA	NA	NA	NA	NA	NA
	Mixture Diff 6mbar	NA	NA	NA	NA	NA	NA
	Mixture Sing 6mbar	165	91	197	109	9,4	1,00
Exp 4	Diff 6mbar						
	Sing 6mbar	174	97	69	95	18,1	1,25
	Mixture Diff 6mbar	NA	NA	NA	NA	NA	NA
	Mixture Sing 6mbar	NA	NA	NA	NA	NA	NA

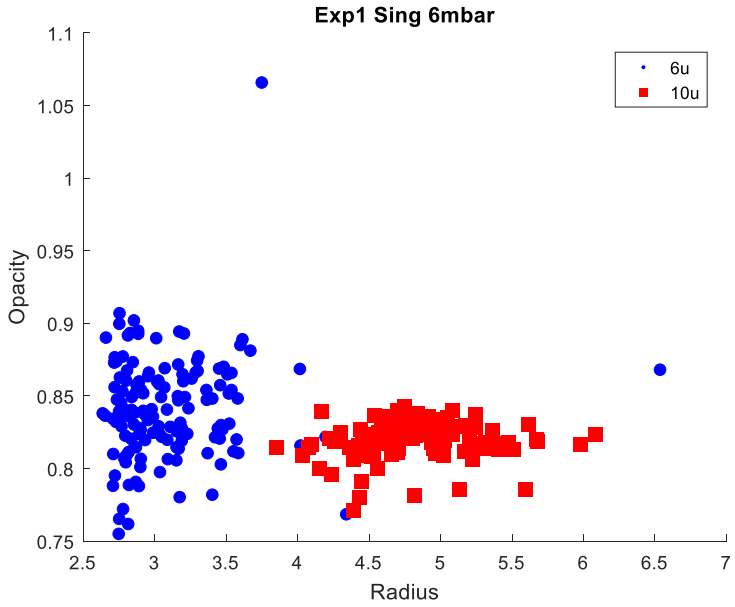

Figure 4.13 An example PDMS-Glass Device Opacity vs Radius Scatter Plot

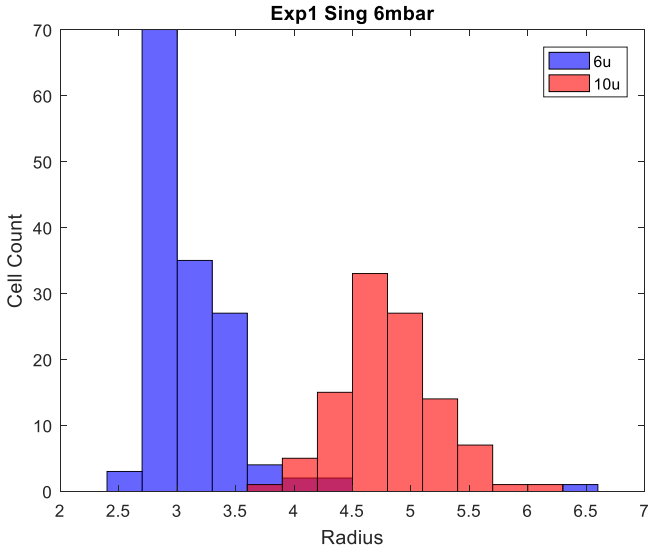

Figure 4.14 An Example Histogram of PDMS-Glass Device Calculated Radiuses

As it is mentioned, beads also passed through the channel in 1:1 mixture solution. For analysis of them, during the data acquisition, same number of beads passed through the channel is assumed. An example mixture result is given in Figure 4.15-16. From the plots, two beads can be distinguished from each other. So, it can be said

that without knowing the certain number of each bead group, separation between them is achieved.

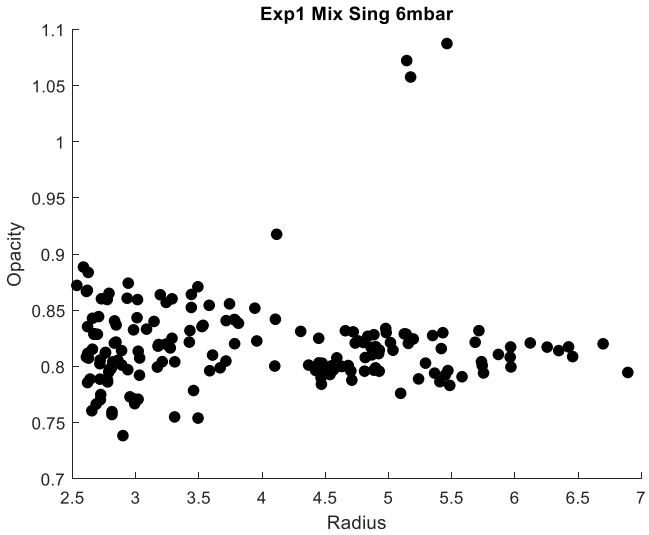

Figure 4.15 An example PDMS-Glass Device Opacity vs Radius Scatter Plot – Mixture

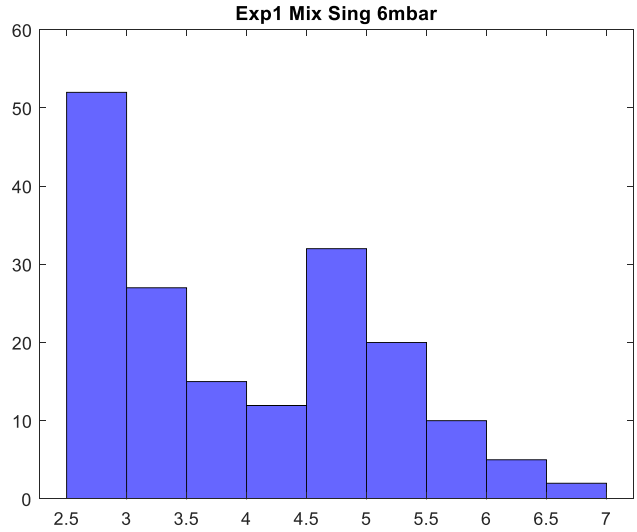

Figure 4.16 An Example Histogram of PDMS-Glass Device Calculated Radiuses – Mixture

In addition to this, during same trials also measurement with higher flow rates are acquired and analyzed on some occasions. Results of them are presented in Table 4.3.

Table 4.3 PDMS-Glass Device - Type 3 - Bead Experiment Results - Different Flow Rates

		# True Detected 6u	% True Detected 6u	# True Detected 10u	% True Detected 10u	% Std.Dev/Mean	Kavg
Exp 1	Diff 10mbar	36	69	0	0	47,5	0,33
	Sing 10mbar	123	95	125	98	12,9	0,69
	Sing 16mbar	118	94	144	100	10,3	1,03
	Sing 20mbar	149	93	127	100	15,8	0,65
	Sing 40mbar	129	95	282	100	12,6	0,91
	Sing 80mbar	45	83	118	100	25,2	0,37
	Mix Diff 10mbar	76	109	64	91	13,6	0,75
	Mix Diff 16mbar	59	104	55	96	10,1	0,62
	Mix Sing 10mbar	81	92	96	108	9,4	1,12
	Mix Sing 16mbar	70	100	70	100	9,7	0,96
	Mix Sing 20mbar	110	124	67	76	11,0	0,95
	Mix Sing 40mbar	71	97	76	103	10,5	0,82
	Mix Sing 80mbar	45	105	41	95	6,8	1,22
Exp 2	Sing 16mbar	98	91	10	50	19,4	0,16
	Sing 20mbar	113	88	106	42	19,9	0,11
	Sing 40mbar	54	81	27	15	30,2	0,01
	Sing 80mbar	25	60	5	5	26,1	0,20
	Mix Diff 10mbar	34	110	28	90	16,3	0,84
	Mix Diff 16mbar	34	110	28	90	16,3	0,84
	Mix Sing 10mbar	118	117	83	83	12,2	0,71
	Mix Sing 16mbar	101	133	51	67	10,7	0,63
	Mix Sing 20mbar	66	115	49	85	10,3	0,61
	Mix Sing 40mbar	40	121	26	79	12,1	0,77

It can be seen from the results, especially in experiment 1, at single-ended measurements device performance was quite high until 80mbar pressure.

However, in differential measurements increasing flow rate above 10mbar resulted in disappearing of peaks. Device could not detect beads differentially above that level. It is thought be related data acquisition capabilities of the impedance spectroscope. Increasing velocity of beads would have caused the device to detect a peak at two sensing electrodes simultaneously. So, resulted impedances would cancel each other, and no detection of beads would be possible. In the single-ended measurement this is not the case, as long as bead travel enough time above the electrodes to impedance spectroscope to detect, a peak would occur, but their amplitude may be lower at high velocities, because of the fact that at time of detection, only a part of the bead may be at the detection zone, which would decrease the peak amplitude. Example result from higher flow rate experiments are given in 4.17-18

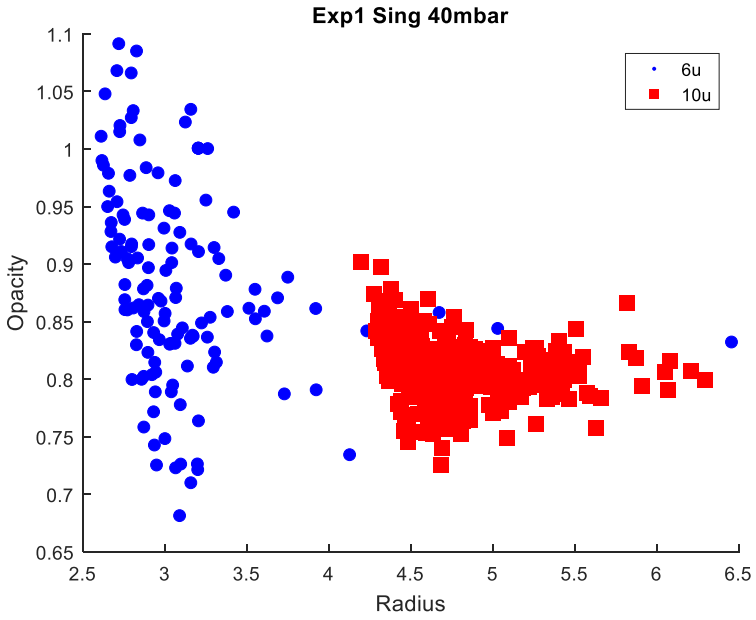

Figure 4.17 An example PDMS-Glass Device Opacity vs Radius Scatter Plot - 40mbar

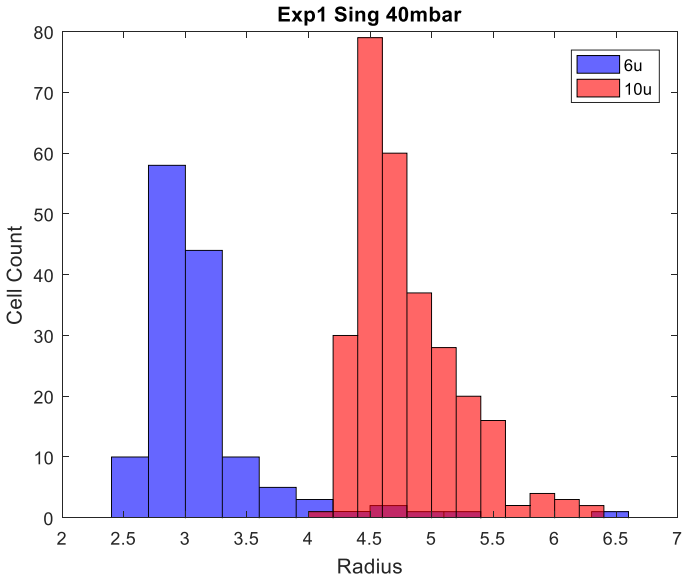

Figure 4.18 An Example Histogram of PDMS-Glass Device Calculated Radiuses – Mixture

4.4.2 Cell Sample Impedance Analysis

Neutrophils and lymphocytes passed through the channel separately and mixed. All experiment analysis process is the same as bead samples.

4.4.2.1 Si-Glass Chip Cell Sample Results

Experiments made on Si-Glass chip using cell samples. Live, magnetically separated lymphocytes and neutrophils used in experiments. They passed through the channel separately and 1:1 and 1:2 mixed. Table 4.4 shows the results from the experiments.

Table 4.4 Si-Glass Live Cell Experiments Results – Separate Passage

		# True Detected Lym	# True Detected Neut	% True Detected Lym	% True Detected Neut	% Std.Dev/Mean	# Total Cell
Exp 1	1-2 Pos.	152	219	89,9	93,2	20,780	0,669
	1-2 Neg.	208	345	83,9	79,7	24,312	0,463
	2-1 Pos.	234	322	79,3	62,2	23,829	0,302
	2-1 Neg.	215	256	84,3	78,5	20,902	0,465
	1 short	131	243	68,6	61,1	21,639	0,236
	1 long	118	277	79,2	66,7	15,610	0,297
	2 short	150	65	63,6	39,2	21,134	0,104
	2 long	121	467	84,0	65,6	17,055	0,294
		# True Detected Lym	# True Detected Neut	% True Detected Lym	% True Detected Neut	% Std.Dev/Mean	# Total Cell
Exp 2	1-2 Pos.	231	263	87,5	88,6	25,461	0,575
	1-2 Neg.	179	125	91,3	100,0	22,485	0,875
	2-1 Pos.	159	88	73,3	50,9	28,725	0,221
	2-1 Neg.	77	85	59,7	28,5	24,181	0,099
	1 short	113	171	64,2	48,4	18,441	0,052
	1 long	38	40	86,4	87,0	23,013	0,356
	2 short	107	145	69,0	43,5	22,127	0,043
	2 long	28	28	82,4	60,9	13,036	0,301
		# True Detected Lym	# True Detected Neut	% True Detected Lym	% True Detected Neut	% Std.Dev/Mean	# Total Cell
Exp 3	1-2 Pos.	99	185	94,3	84,5	24,291	0,440
	1-2 Neg.	341	437	89,3	81,5	22,321	0,510
	2-1 Pos.	239	248	80,7	69,9	23,190	0,316
	2-1 Neg.	693	475	82,1	80,5	26,061	0,437
	1 short	396	346	72,0	58,1	21,466	0,215
	1 long	148	169	82,2	69,0	14,030	0,350
	2 short	383	499	69,1	60,4	22,449	0,263
	2 long	131	163	86,2	69,7	15,148	0,375
		# True Detected Lym	# True Detected Neut	% True Detected Lym	% True Detected Neut	% Std.Dev/Mean	# Total Cell
Exp 4	1-2 Pos.	29	343	90,6	80,7	19,949	0,553
	1-2 Neg.	93	392	77,5	75,7	20,959	0,428
	2-1 Pos.	77	253	75,5	65,9	36,047	0,304
	2-1 Neg.	158	362	81,0	84,6	38,832	0,479
	1 short	100	281	61,0	49,7	23,223	0,096
	1 long	17	45	77,3	60,8	28,469	0,169
	2 short	155	196	76,7	64,3	23,036	0,326
	2 long	10	30	58,8	50,8	20,101	0,139
		# True Detected Lym	# True Detected Neut	% True Detected Lym	% True Detected Neut	% Std.Dev/Mean	# Total Cell
Exp 5	1-2 Pos.	200	345	69,2	53,8	25,989	0,199
	1-2 Neg.	107	226	64,8	55,8	20,036	0,172
	2-1 Pos.	109	228	68,1	46,4	23,529	0,141
	2-1 Neg.	50	102	70,4	58,0	19,364	0,222
	1 short	205	233	68,1	59,4	28,084	0,151
	1 long	43	94	91,5	70,1	10,600	0,458
	2 short	113	311	55,7	37,9	32,570	0,027
	2 long	19	49	100,0	80,3	7,353	0,540

Table 4.4 shows that there are results that show good detection and distinction, however there are also some results that nearly as good. Possible reasons of this issue are discussed in previous sections.

As it is mentioned also mixture experiments with live cells are conducted. 1:1 and 1:2 lymphocyte to neutrophil mixtures are used. Results of them are given in Table 4.5.

Table 4.5 Si-Glass Live Cell Experiments Results – Mixed Passage 1:1 1:2

		# True Detected Lym	# True Detected Neut	% True Detected Lym	% True Detected Neut	% Std.Dev/Mean	# Total Cell
Exp 1 1:1	1-2 Pos.	4	9	61,5	138,5	0,573	13
	1-2 Neg.	59	49	109,3	90,7	0,972	108
	2-1 Pos.	116	120	98,3	101,7	0,965	236
	2-1 Neg.	158	194	89,8	110,2	0,882	352
	1 short	125	86	118,5	81,5	1,526	211
	1 long	55	68	89,4	110,6	0,697	123
	2 short	155	139	105,4	94,6	1,192	294
	2 long	57	60	97,4	102,6	0,537	117
		# True Detected Lym	# True Detected Neut	% True Detected Lym	% True Detected Neut	% Std.Dev/Mean	# Total Cell
Exp 3 1:1	1-2 Pos.	10	12	90,9	109,1	0,764	22
	1-2 Neg.	9	10	94,7	105,3	0,707	19
	2-1 Pos.	7	5	116,7	83,3	0,607	12
	2-1 Neg.	0	1	0,0	200,0	0,000	1
	1 short	216	293	84,9	115,1	0,868	509
	1 long	49	61	89,1	110,9	0,686	110
	2 short	72	72	100,0	100,0	1,043	144
	2 long	28	24	107,7	92,3	0,575	52
		# True Detected Lym	# True Detected Neut	% True Detected Lym	% True Detected Neut	% Std.Dev/Mean	# Total Cell
Exp 5 1:1	1-2 Pos.	74	79	96,7	103,3	0,427	153
	1-2 Neg.	87	103	91,6	108,4	0,534	190
	2-1 Pos.	97	92	102,6	97,4	0,450	189
	2-1 Neg.	96	93	101,6	98,4	0,430	189
	1 short	240	218	104,8	95,2	0,627	458
	1 long	16	17	97,0	103,0	0,370	33
	2 short	173	181	97,7	102,3	0,508	354
	2 long	0	0	0,0	0,0	0,000	0
		# True Detected Lym	# True Detected Neut	% True Detected Lym	% True Detected Neut	% Std.Dev/Mean	# Total Cell
Exp 2 1:2	1-2 Pos.	19	19	150,0	75,0	1,050	38
	1-2 Neg.	27	35	130,6	84,7	0,777	62
	2-1 Pos.	49	63	131,3	84,4	1,129	112
	2-1 Neg.	99	165	112,5	93,8	0,936	264
	1 short	147	123	163,3	68,3	1,254	270
	1 long	15	21	125,0	87,5	1,179	36
	2 short	189	227	136,3	81,9	0,992	416
	2 long	30	62	97,8	101,1	0,758	92
		# True Detected Lym	# True Detected Neut	% True Detected Lym	% True Detected Neut	% Std.Dev/Mean	# Total Cell
Exp 4 1:2	1-2 Pos.	49	78	115,7	92,1	0,741	127
	1-2 Neg.	13	20	118,2	90,9	0,662	33
	2-1 Pos.	2	5	85,7	107,1	0,337	7
	2-1 Neg.	7	6	161,5	69,2	0,698	13
	1 short	149	240	114,9	92,5	0,814	389
	1 long	39	64	113,6	93,2	0,573	103
	2 short	252	324	131,3	84,4	0,844	576
	2 long	19	55	77,0	111,5	0,627	74
		# True Detected Lym	# True Detected Neut	% True Detected Lym	% True Detected Neut	% Std.Dev/Mean	# Total Cell
Exp 6 1:2	1-2 Pos.	11	17	117,9	91,1	0,764	28
	1-2 Neg.	37	51	126,1	86,9	0,618	88
	2-1 Pos.	26	43	113,0	93,5	0,480	69
	2-1 Neg.	53	109	98,1	100,9	0,413	162
	1 short	249	337	127,5	86,3	0,869	586
	1 long	38	61	115,2	92,4	0,510	99
	2 short	93	143	118,2	90,9	0,542	236
	2 long	25	28	141,5	79,2	0,504	53

Same issue with previous experiments continues here. There are good results however they are not fully repeatable.

Example results of them are given in Figure 4.19-22.

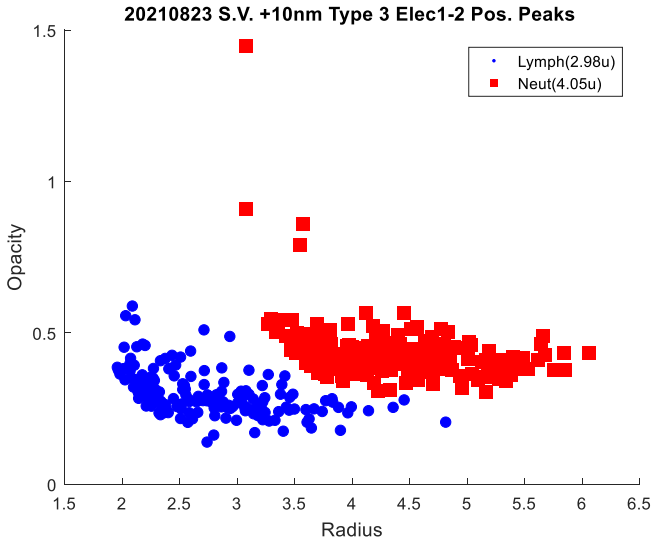

Figure 4.19 An example Si-Glass Device Opacity vs Radius Scatter Plot - Live Cells - Separate

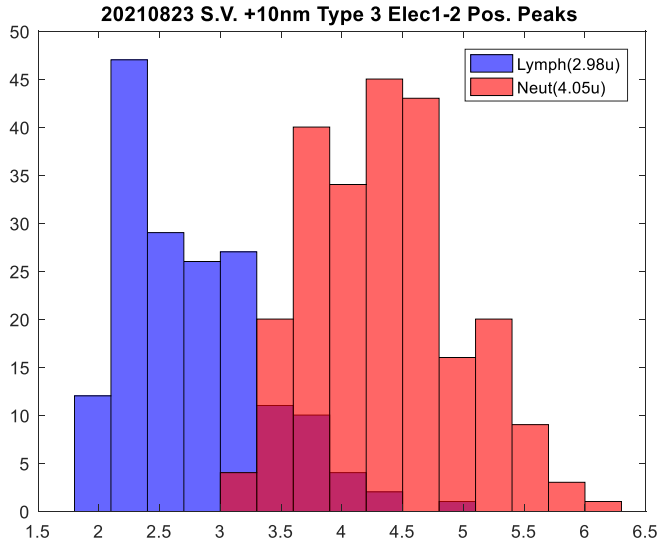

Figure 4.20 An Example Histogram of Si-Glass Device Calculated Radiuses – Live Cells - Separate

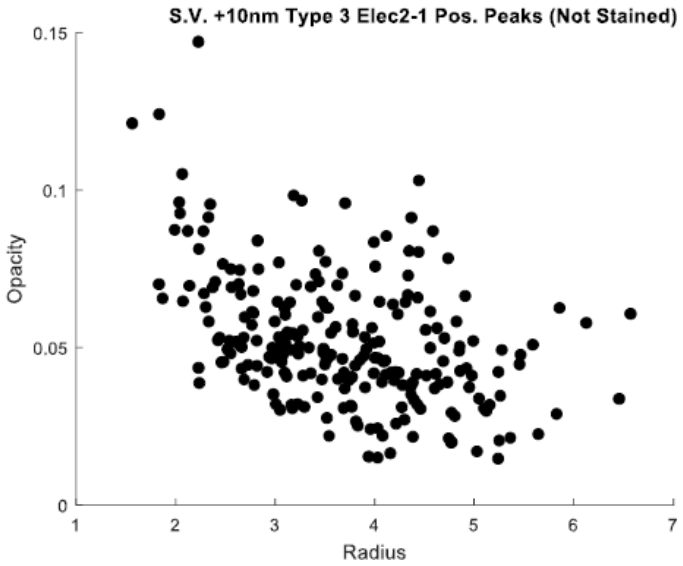

Figure 4.21 An example Si-Glass Device Opacity vs Radius Scatter Plot - Live Cells - 1:1 Mix

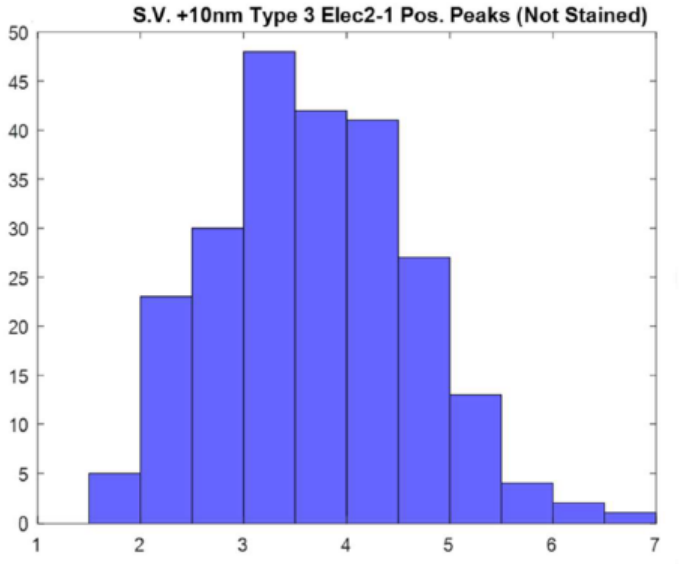

Figure 4.22 An Example Histogram of Si-Glass Device Calculated Radiuses – Live Cells - 1:1 Mix

4.4.2.2 PDMS-Glass Chip Cell Sample Results

Experiments made on PDMS-Glass chip using fixed lymphocyte and neutrophil cell samples. Experimental procedures are same with other experiment groups. Results are provided in Table 4.6.

Table 4.6 PDMS-Glass Live Cell Experiments Results – Separate- Mixed Passage

		# True Detected Lymph	% True Detected Lymph	# True Detected Neut	% True Detected Neut	% Std.Dev/Mean	Resolution
Exp 1	Diff 6mbar	158	69	69	47	22,8	0,09
	Sing 6mbar	151	68	196	47	16,2	0,08
	Diff 6mbar Mix	189	112	119	86	12,1	0,64
	Sing 6mbar Mix	172	108	117	90	8,8	0,78
Exp 2	Diff 6mbar	187	59	79	35	21,6	0,05
	Sing 6mbar	111	70	80	49	24,9	0,06
	Diff 6mbar Mix	151	99	87	102	15,8	0,55
	Sing 6mbar Mix	197	89	148	119	10,3	0,68
Exp 3	Diff 6mbar	124	77	168	52	16,2	0,17
	Sing 6mbar	284	80	381	60	16,4	0,24
	Diff 6mbar Mix	261	98	222	102	9,3	0,62
	Sing 6mbar Mix	324	97	285	104	8,9	0,68
Exp 4	Diff 6mbar	160	73	92	47	21,2	0,09
	Sing 6mbar	208	77	190	65	12,2	0,29
	Diff 6mbar Mix	83	146	52	66	10,5	0,58
	Sing 6mbar Mix	176	131	145	78	9,4	0,68
Exp 4	Sing 6mbar	164	89	122	80	16	0,43
	Mix Sing 6mbar	85	112	67	88	10	0,83

Results are also similar in PDMS-Glass device. There is a repeatability problem.

Example plots are for PDMS-Glass cell experiments is provided in Figure 4.23-24.

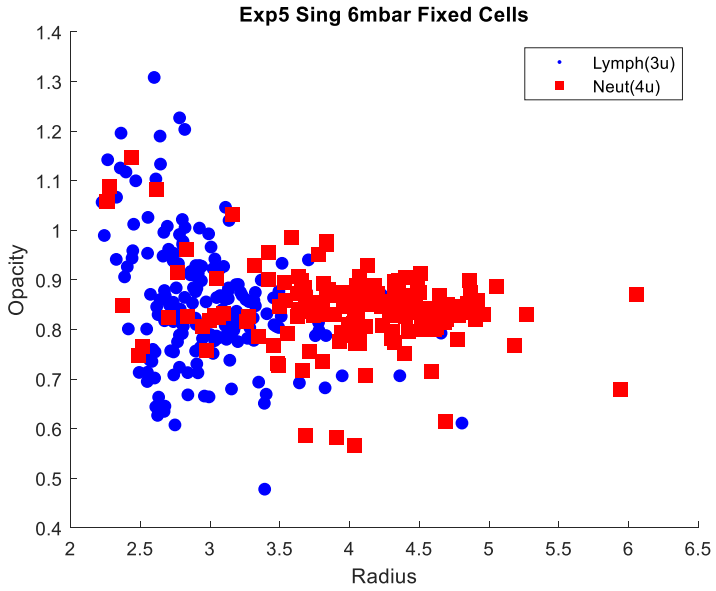

Figure 4.23 An example PDMS-Glass Device Opacity vs Radius Scatter Plot - Fixed Cells - Separate

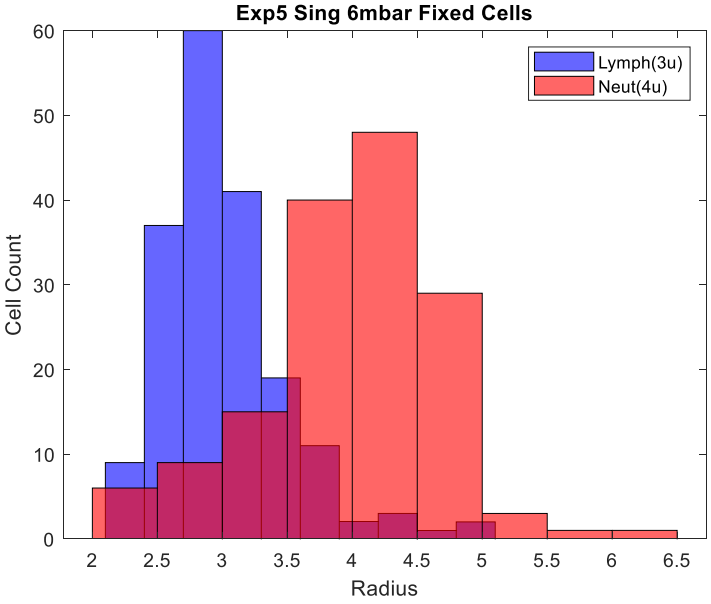

Figure 4.24 An Example Histogram of Si-Glass Device Calculated Radiuses – Fixed Cells – Separate

4.5 Chip Cartridge Test Results

Chip cartridge tests are made to check compatibility of the device with the chip cartridge. First parameter to be checked with these tests is sealing of the chip cartridge. Cartridge should seal properly the chip and prevent leakage out of the chip and cartridge. After sealing is secured then healthy fluid flow through the chip should be checked. Since existing chip cartridge reservoir for chip is shallow, long bolts and nuts is used to secure the PDMS-Glass device between two cartridge parts. Photo of secured chip is given in Figure 4.15.

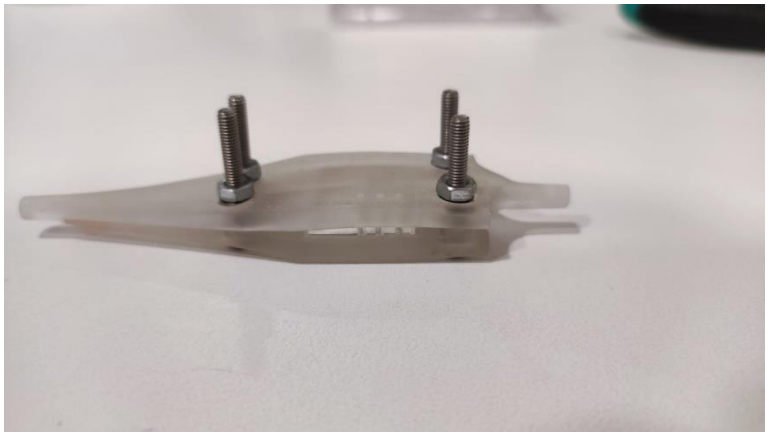

Figure 4.25 Secured Chip inside Chip Cartridge

Then using a vacuum source and regulator, DI water flow through the system is checked. Used setup for this test is given in Figure 4.16. During the test fluid flow through the system is achieved without leakage through the cartridge.

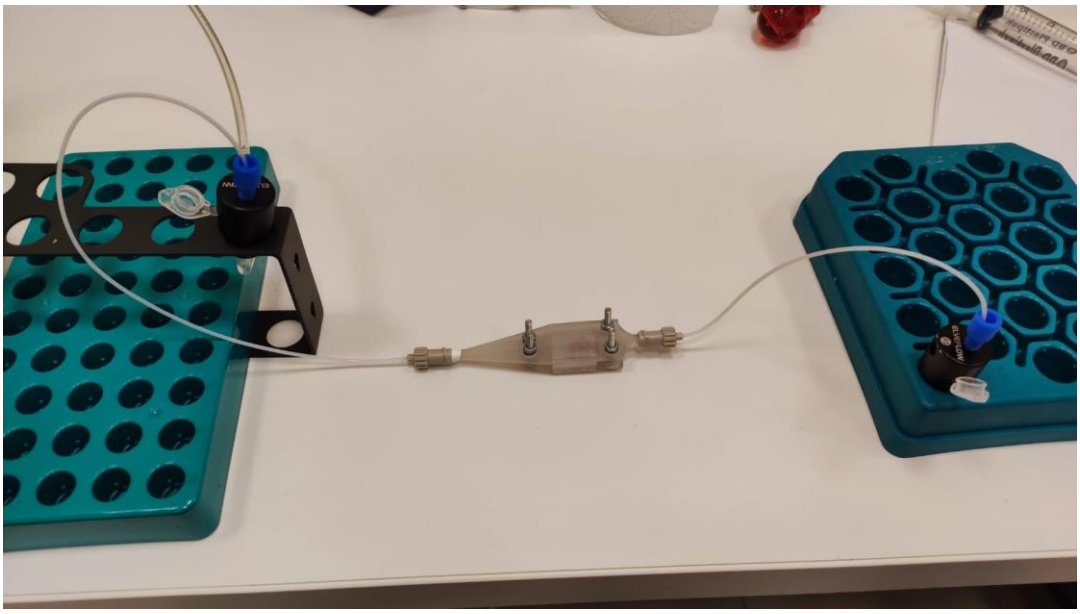

Figure 4.26 Chip Cartridge Test Setup with Vacuum Regulator

CHAPTER 5

CONCLUSION AND OUTLOOK

The main objective of this study was to develop an impedance flow cytometry system that is to be used for differentiate and count main white blood cell subtypes; neutrophil and lymphocytes. This developed IFC chip is aimed to be part of a portable cell counter device, so implementation of this chip with cartridge that is designed to be used with this device was the second goal of this study. To achieve these objectives, device design, design validation, fabrication and experimental validation studies were carried out.

The achievements are summarized below:

- Existing IFC device design was validated using simulations. Simulation results are verified experimentally.
- PDMS mold for fabrication of microchannel is achieved and PDMS-Glass device is fabricated.
- Experimental setup and protocol were developed and verified with successful experiments.
- Peak detection algorithm is developed and used to analyze experimental data.
- Device performance is characterized using bead experiments. Successful count and differentiation of beads achieved at experiments. Possible reasons of unsuccessful experiments are discussed.
- Live and fixed cell experiments are made with lymphocytes and neutrophils separated from whole blood. Results show successful differentiation and counting is achieved with IFC device. Possible reasons for unsuccessful experiments are discussed.
- Implementation of IFC chip with chip cartridge is achieved. Successful flow through the chip inside the chip cartridge is achieved.

Considering the research objectives and achievements mentioned, it can be said that the objectives of thesis were met to a certain level. Repeatability of experiments was the main issue that is encountered during this thesis study. To solve this issue IFC device design may be changed from coplanar electrode configuration to parallel electrode configuration. Since, the most probable reason for repeatability issue was thought as dispersion of beads/cells position along the height of the channel. Changing electrode configuration to parallel would diminish the z position dependency of the impedance of cell/bead. Alternatively, a focusing may be included without changing the electrode configuration to limit cells dispersion along z axis. In addition to these improvements, obtained data may be refined further with signal processing applications to obtain better results from the same data [52].

REFERENCES

[1] M. Hutchings, A. Truman, and B. Wilkinson, “Antibiotics: past, present and future,” *Curr Opin Microbiol*, vol. 51, pp. 72–80, Oct. 2019, doi: 10.1016/J.MIB.2019.10.008.

[2] M. Frieri, K. Kumar, and A. Boutin, “Antibiotic resistance,” *J Infect Public Health*, vol. 10, no. 4, pp. 369–378, Jul. 2017, doi: 10.1016/J.JIPH.2016.08.007.

[3] K. Bush *et al.*, “Tackling antibiotic resistance,” *Nature Reviews Microbiology 2011 9:12*, vol. 9, no. 12, pp. 894–896, Nov. 2011, doi: 10.1038/nrmicro2693.

[4] T. P. van Boeckel *et al.*, “Global antibiotic consumption 2000 to 2010: an analysis of national pharmaceutical sales data,” *Lancet Infect Dis*, vol. 14, no. 8, pp. 742–750, Aug. 2014, doi: 10.1016/S1473-3099(14)70780-7.

[5] Gartner Leslie, “Textbook of Hystology,” pp. 459–486, 2020.

[6] T. Zhou, N. Zheng, X. Li, D. Zhu, and Y. Han, “Prognostic value of neutrophil- lymphocyte count ratio (NLCR) among adult ICU patients in comparison to APACHE II score and conventional inflammatory markers: a multi center retrospective cohort study,” *BMC Emerg Med*, vol. 21, no. 1, Dec. 2021, doi: 10.1186/S12873-021-00418-2.

[7] M. Karawajczyk, S. Haile, M. Grabski, and A. Larsson, “The HemoCue WBC DIFF system could be used for leucocyte and neutrophil counts but not for full differential counts,” *Acta Paediatr*, vol. 106, no. 6, pp. 974–978, Jun. 2017, doi: 10.1111/APA.13790.

[8] D. S. Chabot-Richards and T. I. George, “White Blood Cell Counts. Reference Methodology.,” *Clin Lab Med*, vol. 35, no. 1, pp. 11–24, Mar. 2015, doi: 10.1016/j.cll.2014.10.007.

[9] I. T. Young, “The Classification of White Blood Cells,” *IEEE Trans Biomed Eng*, vol. BME-19, no. 4, pp. 291–298, 1972, doi: 10.1109/TBME.1972.324072.

[10] K. J. Halazun *et al.*, “Negative impact of neutrophil-lymphocyte ratio on outcome after liver transplantation for hepatocellular carcinoma,” *Ann Surg*, vol. 250, no. 1, pp. 141–151, Jul. 2009, doi: 10.1097/SLA.0B013E3181A77E59.

[11] B. D. Horne *et al.*, “Which White Blood Cell Subtypes Predict Increased Cardiovascular Risk?,” *J Am Coll Cardiol*, vol. 45, no. 10, pp. 1638–1643, May 2005, doi: 10.1016/J.JACC.2005.02.054.

[12] S. L. Shao, H. Y. Cong, M. Y. Wang, and P. Liu, “The diagnostic roles of neutrophil in bloodstream infections,” *Immunobiology*, vol. 225, no. 1, Jan. 2020, doi: 10.1016/J.IMBIO.2019.10.007.

[13] S. Nazlibilek, D. Karacor, T. Ercan, M. H. Sazli, O. Kalender, and Y. Ege, “Automatic segmentation, counting, size determination and classification of white blood cells,” *Measurement (Lond)*, vol. 55, pp. 58–65, 2014, doi: 10.1016/J.MEASUREMENT.2014.04.008.

[14] T. Honda, T. Uehara, G. Matsumoto, S. Arai, and M. Sugano, “Neutrophil left shift and white blood cell count as markers of bacterial infection,” *Clinica Chimica Acta*, vol. 457, pp. 46–53, Jun. 2016, doi: 10.1016/J.CCA.2016.03.017.

[15] M. Holub, O. Beran, N. Kaspříková, and P. Chalupa, “Neutrophil to lymphocyte count ratio as a biomarker of bacterial infections,” *Cent Eur J Med*, vol. 7, no. 2, pp. 258–261, Apr. 2012, doi: 10.2478/S11536-012-0002-3/MACHINEREADABLECITATION/RIS.

[16] A. L. Mescher, L. C. U. Junqueira, and A. L. Preceded by: Mescher, “Junqueira’s basic histology : text and atlas”.

[17] M. Absher, “Hemocytometer Counting,” *Tissue Culture*, pp. 395–397, Jan. 1973, doi: 10.1016/B978-0-12-427150-0.50098-X.

[18] B. C. Morten, R. J. Scott, and K. A. Avery-Kiejda, “Comparison of three different methods for determining cell proliferation in breast cancer cell lines,” *Journal of Visualized Experiments*, vol. 2016, no. 115, Sep. 2016, doi: 10.3791/54350.

[19] M. J. A. Martín, L. A. Queral, L. S. Frías, L. V. Amado, A. Merino, and L. G. de Guadiana-Romualdo, “Automated cell count in body fluids: A review,” *Advances in Laboratory Medicine*, vol. 2, no. 2, pp. 149–161, Jun. 2021, doi: 10.1515/ALMED-2021-0011/ASSET/GRAPHIC/J_ALMED-2021-0011_FIG_001.JPG.

[20] “TC20 Automated Cell Counter | Bio-Rad.” https://www.bio-rad.com/en-tr/product/tc20-automated-cell-counter?ID=M7FBG34VY (accessed Jan. 20, 2023).

[21] K. M. McKinnon, “Flow Cytometry: An Overview,” *Curr Protoc Immunol*, vol. 120, no. 1, pp. 5.1.1-5.1.11, Jan. 2018, doi: 10.1002/CPIM.40.

[22] A. Adan, G. Alizada, Y. Kiraz, Y. Baran, and A. Nalbant, “Flow cytometry: basic principles and applications,” *Crit Rev Biotechnol*, vol. 37, no. 2, pp. 163–176, Feb. 2017, doi: 10.3109/07388551.2015.1128876.

[23] W. H. Coulter, “High speed automatic blood cell counter and cell size analyzer,” in *Proceedings of the National Electronics Conference*, 1956, p. 1034.

[24] T. Sun and H. Morgan, “Single-cell microfluidic Impedance cytometry: A review,” *Microfluidics and Nanofluidics*, vol. 8, no. 4. pp. 423–443, Apr. 2010. doi: 10.1007/s10404-010-0580-9.

[25] J. Hurley, “Sizing Particles with a Coulter Counter,” *Biophys J*, vol. 10, no. 1, pp. 74–79, 1970, doi: 10.1016/S0006-3495(70)86286-5.

[26] K. C. Cheung *et al.*, “Microfluidic impedance-based flow cytometry,” *Cytometry Part A*, vol. 77, no. 7. pp. 648–666, Jul. 2010. doi: 10.1002/cyto.a.20910.

[27] S. Gawad, L. Schild, and P. Renaud, “Micromachined impedance spectroscopy flow cytometer for cell analysis and particle sizing,” *Lab Chip*, vol. 1, no. 1, pp. 76–82, Sep. 2001, doi: 10.1039/b103933b.

[28] K. Cheung, S. Gawad, and P. Renaud, “Impedance spectroscopy flow cytometry: On-chip label-free cell differentiation,” *Cytometry Part A*, vol. 65, no. 2, pp. 124–132, Jun. 2005, doi: 10.1002/CYTO.A.20141.

[29] H. Morgan, T. Sun, D. Holmes, S. Gawad, and N. G. Green, “Single cell dielectric spectroscopy,” *J Phys D Appl Phys*, vol. 40, no. 1, pp. 61–70, Jan. 2007, doi: 10.1088/0022-3727/40/1/S10.

[30] T. Sun, N. G. Green, and H. Morgan, “Analytical and numerical modeling methods for impedance analysis of single cells on-chip,” *Nano*, vol. 3, no. 1, pp. 55–63, Feb. 2008, doi: 10.1142/S1793292008000800.

[31] J. C. Maxwell, “A treatise on electricity and magnetism.,” 1954.

[32] K. R. Foster and H. P. Schwan, “Dielectric properties of tissues and biological materials: a critical review,” *Crit Rev Biomed Eng*, vol. 17, no. 1, pp. 25–104, 1989, Accessed: Jan. 22, 2023. [Online]. Available: https://pubmed.ncbi.nlm.nih.gov/2651001/

[33] K. H. Schoenbach *et al.*, “Bioelectric effects of intense nanosecond pulses,” *IEEE Transactions on Dielectrics and Electrical Insulation*, vol. 14, no. 5, pp. 1088–1107, Oct. 2007, doi: 10.1109/TDEI.2007.4339468.

[34] T. Sun and H. Morgan, “Single-cell microfluidic Impedance cytometry: A review,” *Microfluidics and Nanofluidics*, vol. 8, no. 4. pp. 423–443, Apr. 2010. doi: 10.1007/s10404-010-0580-9.

[35] Y. Feng, L. Huang, P. Zhao, F. Liang, and W. Wang, “A Microfluidic Device Integrating Impedance Flow Cytometry and Electric Impedance Spectroscopy for High-Efficiency Single-Cell Electrical Property Measurement,” *Anal Chem*, vol. 91, no. 23, pp. 15204–15212, Dec. 2019, doi: 10.1021/ACS.ANALCHEM.9B04083/SUPPL_FILE/AC9B04083_SI_004.AVI.

[36] A. de Ninno, V. Errico, F. R. Bertani, L. Businaro, P. Bisegna, and F. Caselli, “Coplanar electrode microfluidic chip enabling accurate sheathless impedance cytometry,” *Lab Chip*, vol. 17, no. 6, pp. 1158–1166, Mar. 2017, doi: 10.1039/C6LC01516F.

[37] D. S. de Bruijn, K. F. A. Jorissen, W. Olthuis, and A. van den Berg, “Determining particle size and position in a coplanar electrode setup using measured opacity for microfluidic cytometry,” *Biosensors (Basel)*, vol. 11, no. 10, p. 353, Oct. 2021, doi: 10.3390/BIOS11100353/S1.

[38] C. Petchakup, P. E. Hutchinson, H. M. Tay, S. Y. Leong, K. H. H. Li, and H. W. Hou, “Label-free quantitative lymphocyte activation profiling using microfluidic impedance cytometry,” *Sens Actuators B Chem*, vol. 339, p. 129864, Jul. 2021, doi: 10.1016/J.SNB.2021.129864.

[39] H. Daguerre, M. Solsona, J. Cottet, M. Gauthier, P. Renaud, and A. Bolopion, “Positional dependence of particles and cells in microfluidic electrical impedance flow cytometry: Origin, challenges and opportunities,” *Lab on a Chip*, vol. 20, no. 20. Royal Society of Chemistry, pp. 3665–3689, Oct. 21, 2020. doi: 10.1039/d0lc00616e.

[40] V. Errico, A. de Ninno, F. R. Bertani, L. Businaro, P. Bisegna, and F. Caselli, “Mitigating positional dependence in coplanar electrode Coulter-type microfluidic devices,” *Sens Actuators B Chem*, vol. 247, pp. 580–586, 2017, doi: 10.1016/J.SNB.2017.03.035.

[41] Y. Zare and K. Y. Rhee, “Experimental data and modeling of electrical conductivity for polymer carbon nanotubes nanobiosensor during degradation in neutral phosphate-buffered saline (PBS),” *Materials Science and Engineering: B*, vol. 252, p. 114482, Feb. 2020, doi: 10.1016/J.MSEB.2019.114482.

[42] D. Holmes, J. K. She, P. L. Roach, and H. Morgan, “Bead-based immunoassays using a micro-chip flow cytometer,” *Lab Chip*, vol. 7, no. 8, pp. 1048–1056, Jul. 2007, doi: 10.1039/B707507N.

[43] B. Şahin, “DESIGN OF A MICROFLUIDIC PLATFORM FOR REAL-TIME ENUMERATION AND RETRIEVAL OF LOW CONCENTRATION OF CELLS A THESIS SUBMITTED TO THE GRADUATE SCHOOL OF NATURAL AND APPLIED SCIENCES OF MIDDLE EAST TECHNICAL UNIVERSITY,” 2022.

[44] Y. Demircan Yalçın *et al.*, “A microfluidic device enabling drug resistance analysis of leukemia cells via coupled dielectrophoretic detection and impedimetric counting,” *Sci Rep*, vol. 11, no. 1, Dec. 2021, doi: 10.1038/S41598-021-92647-5.

[45] J. Chen, C. Xue, Y. Zhao, D. Chen, M. H. Wu, and J. Wang, “Microfluidic impedance flow cytometry enabling high-throughput single-cell electrical property characterization,” *International Journal of Molecular Sciences*, vol. 16, no. 5. MDPI AG, pp. 9804–9830, Apr. 29, 2015. doi: 10.3390/ijms16059804.

[46] S. Gawad, K. Cheung, U. Seger, A. Bertsch, and P. Renaud, “Dielectric spectroscopy in a micromachined flow cytometer: Theoretical and practical considerations,” *Lab Chip*, vol. 4, no. 3, pp. 241–251, 2004, doi: 10.1039/b313761a.

[47] M. G. Macey, “Flow cytometry: Principles and applications,” *Flow Cytometry: Principles and Applications*, pp. 1–290, 2007, doi: 10.1007/978-1-59745-451-3/COVER.

[48] S. Emaminejad, M. Javanmard, R. W. Dutton, and R. W. Davis, “Microfluidic diagnostic tool for the developing world: contactless impedance flow cytometry,” *Lab Chip*, vol. 12, no. 21, pp. 4499–4507, Oct. 2012, doi: 10.1039/C2LC40759K.

[49] H. Tan *et al.*, “Inherent bioelectrical parameters of hundreds of thousands of single leukocytes based on impedance flow cytometry,” *Cytometry Part A*, vol. 101, no. 8, pp. 630–638, Aug. 2022, doi: 10.1002/CYTO.A.24544.

[50] H. Song *et al.*, “A microfluidic impedance flow cytometer for identification of differentiation state of stem cells,” *Lab Chip*, vol. 13, no. 12, pp. 2300–2310, May 2013, doi: 10.1039/C3LC41321G.

[51] D. Holmes and H. Morgan, “Single cell impedance cytometry for identification and counting of CD4 T-cells in human blood using impedance labels,” *Anal Chem*, vol. 82, no. 4, pp. 1455–1461, Feb. 2010, doi: 10.1021/AC902568P/ASSET/IMAGES/LARGE/AC-2009-02568P_0001.JPEG.

[52] D. S. de Bruijn, K. F. A. Jorissen, W. Olthuis, and A. van den Berg, “Determining particle size and position in a coplanar electrode setup using measured opacity for microfluidic cytometry,” *Biosensors (Basel)*, vol. 11, no. 10, Oct. 2021, doi: 10.3390/bios11100353.

APPENDICES

Appendix A. Regression Equations

1.

S *R-sq* *R-sq(adj)* *R-sq(pred)*

0.0000001 97.48% 95.58% 89.90%

6max-8min = 0.000000 + 0.00913 z - 0.00283 w - 0.01420 s

2.

z3_s3_z2s_s2z

S *R-sq* *R-sq(adj)* *R-sq(pred)*

0.0000001 98.87% 97.55% 95.29%

8mindev-6maxdev = -0.000000 - 0.0232 z + 0.0587 s + 144 z*z - 1679 s*s + 529 z*s
+ 13556358 s*s*s - 5594555 z*z*s

S *R-sq* *R-sq(adj)* *R-sq(pred)*

0.0000000 93.87% 86.73% 75.04%

8zmiddev-6zmiddev = 0.000001 - 0.0304 z - 0.0161 s + 218 z*z - 53 s*s + 598 z*s
+ 878114 s*s*s - 4884373 z*z*s

s3_z2_s2

S *R-sq* *R-sq(adj)* *R-sq(pred)*

0.0000000 98.85% 97.86% 95.79%

8mindev-6maxdev = -0.000001 - 0.0143 z + 0.0608 s - 3 z*z - 1562 s*s + 193.5 z*s
+ 12130015 s*s*s

S *R-sq* *R-sq(adj)* *R-sq(pred)*

0.0000000 93.76%   88.42%   77.35%

8zmiddev-6zmiddev = 0.000001 - 0.0227 z - 0.0143 s + 89 z*z + 49 s*s + 305.2 z*s

- 367167 s*s*s

z2_s2

S *R-sq* *R-sq(adj)* *R-sq(pred)*

0.0000001 98.41%   97.41%   95.04%

8mindev-6maxdev = -0.000000 - 0.0115 z + 0.03850 s - 51 z*z - 550 s*s + 193.5 z*s

S *R-sq* *R-sq(adj)* *R-sq(pred)*

0.0000000 93.76%   89.86%   78.05%

8zmiddev-6zmiddev = 0.000001 - 0.0227 z - 0.01358 s + 91 z*z + 18.0 s*s + 305.2 z*s

Appendix B. Peak Detection Algorithm MATLAB Code

Scatter Plot – Histogram Generation

```
close all

LymRad = 3;
NeutRad = 4;


HF6 = data6(:,2);
HF10 = data10(:,2);
LF6 = data6(:,1);
LF10 = data10(:,1);
LF6_3 = LF6.^(1/3);
LF10_3 = LF10.^(1/3);
LF6_avg = mean(LF6_3);
LF10_avg = mean(LF10_3);
Tot6 = length(LF6_3);
Tot10 = length(LF10_3);
K6 = LF6_avg/LymRad;
K10 = LF10_avg/NeutRad;
Kavg = (K6+K10)/2;
Kavg_weight = ((K6*Tot6)+(K10*Tot10))/(Tot6+Tot10);
Rad6 = LF6_3/Kavg;
Rad10 = LF10_3/Kavg;
Opac6 = HF6./LF6;
Opac10 = HF10./LF10;

check6 = Rad6 <= (LymRad+NeutRad)/2;

check10 = Rad10 >= (LymRad+NeutRad)/2;

RadBelow = Rad6(check6);
RadAbove = Rad10(check10);


TrueRad6 = sum(check6(:) == 1);

TrueRad10 = sum(check10(:) == 1);

TotalRad6 = length(Rad6);
TotalRad10 = length(Rad10);

TrueRad6_Percent = (TrueRad6/TotalRad6)*100;
TrueRad10_Percent = (TrueRad10/TotalRad10)*100;


Mean6 = mean(Rad6);
Mean10 = mean(Rad10);
std6 = std(Rad6);
```

```
std10 = std(Rad10);
stdmean6 = (std6/Mean6)*100;
stdmean10 = (std10/Mean10)*100;
stdmeanavg = (stdmean6+stdmean10)/2;
Reso = abs((Mean6-Mean10)/(0.5*(4*std6+4*std10)));


Results = [TrueRad6 TrueRad6_Percent TrueRad10 TrueRad10_Percent
stdmeanavg Reso Kavg Kavg_weight];

figure

scatter(Rad6, Opac6, 400, 'blue', '.');

hold on

scatter(Rad10, Opac10, 80, 'red','s','filled');

title('Exp5 Sing 6mbar Fixed Cells');  %CHANGE TITLE ACCORDINGLY

xlabel ('Radius');
ylabel ('Opacity');

% legend ('6u' , '10u')
legend ('Lymph(3u)' , 'Neut(4u)')

figure
histogram (Rad6,'FaceColor','blue');

hold on

histogram (Rad10,'FaceColor','red');

% legend ('6u' , '10u')
legend ('Lymph(3u)' , 'Neut(4u)')

xlabel ('Radius');
ylabel ('Cell Count');

title('Exp5 Sing 6mbar Fixed Cells');   %CHANGE TITLE ACCORDINGLY
```

Peak Detection Code – GitHub QR Code